

Changes to Peroxyacyl Nitrates (PANs) over Megacities in Response to COVID-19 Tropospheric NO₂ Reductions Observed by the Cross-track Infrared Sounder (CrIS)

Madison Jane Shogrin¹, Vivienne H. Payne², Susan Kulawik³, Kazuyuki Miyazaki⁴, and Emily V Fischer¹

¹Colorado State University

²Jet Propulsion Laboratory, California Institute of Technology

³NASA Ames Research Center

⁴Jet Propulsion Laboratory

October 26, 2023

Abstract

The COVID-19 pandemic perturbed air pollutant emissions as cities shutdown worldwide. Peroxyacyl nitrates (PANs) are important tracers of photochemistry that are formed through the oxidation of non-methane volatile organic compounds (NMVOCs) in the presence of nitrogen oxide radicals (NO_x = NO + NO₂). We use satellite measurements of free tropospheric PANs from the S-NPP Cross-Track Infrared Sounder (CrIS) over eight of the world's megacities: Mexico City, Beijing, Los Angeles, Tokyo, São Paulo, Delhi, Lagos, and Karachi. We quantify the seasonal cycle of PANs over these megacities and find seasonal maxima in PANs correspond to seasonal peaks in local photochemistry. CrIS is used to explore changes in PANs in response to the COVID-19 lockdowns. Statistically significant changes to PANs occurred over two megacities: Los Angeles (PAN decreased) and Beijing (PAN increased). Our analysis suggests that large perturbations in NO_x may not result in significant declines in NO_x export potential of megacities.

Hosted file

965311_0_supp_11058066_rvw7m1.docx available at <https://authorea.com/users/665994/articles/667016-changes-to-peroxyacyl-nitrates-pans-over-megacities-in-response-to-covid-19-tropospheric-no2-reductions-observed-by-the-cross-track-infrared-sounder-cris>

1 **Changes to Peroxyacyl Nitrates (PANs) over Megacities in Response to COVID-19**
2 **Tropospheric NO₂ Reductions Observed by the Cross-track Infrared Sounder (CrIS)**
3 **Madison J. Shogrin¹, Vivienne H. Payne², Susan S. Kulawik³, Kazuyuki Miyazaki², and**
4 **Emily V. Fischer¹**

5 ¹Colorado State University, Department of Atmospheric Science, Fort Collins, CO, USA.

6 ²Jet Propulsion Laboratory, California Institute of Technology, Pasadena CA, USA.

7 ³Bay Area Environmental Research Institute, Petaluma, CA, USA.

8 Corresponding author: Madison J. Shogrin (madison.shogrin@colostate.edu)

9 **Key Points:**

- 10 • There are pronounced seasonal cycles of PANs over each megacity that align with
11 seasonal maximums in photochemistry.
- 12 • Observed free tropospheric mixing ratios of PANs during COVID-19 were significantly
13 different over two out of eight surveyed megacities.
- 14 • Sensitivity of free tropospheric PANs to the abundance of precursors is seasonally
15 dependent in some locations.

16 Abstract

17 The COVID-19 pandemic perturbed air pollutant emissions as cities shutdown worldwide. Peroxyacyl
18 nitrates (PANs) are important tracers of photochemistry that are formed through the oxidation of non-
19 methane volatile organic compounds (NMVOCs) in the presence of nitrogen oxide radicals ($\text{NO}_x = \text{NO} +$
20 NO_2). We use satellite measurements of free tropospheric PANs from the S-NPP Cross-Track Infrared
21 Sounder (CrIS) over eight of the world's megacities: Mexico City, Beijing, Los Angeles, Tokyo, São
22 Paulo, Delhi, Lagos, and Karachi. We quantify the seasonal cycle of PANs over these megacities and find
23 seasonal maxima in PANs correspond to seasonal peaks in local photochemistry. CrIS is used to explore
24 changes in PANs in response to the COVID-19 lockdowns. Statistically significant changes to PANs
25 occurred over two megacities: Los Angeles (PAN decreased) and Beijing (PAN increased). Our analysis
26 suggests that large perturbations in NO_x may not result in significant declines in NO_x export potential of
27 megacities.

28 Plain Language Summary

29 The COVID-19 pandemic led to the lockdown of urban centers worldwide, drastically perturbing the
30 concentrations of global air pollutants. Peroxyacyl nitrates (PANs) are important photochemical
31 pollutants formed from reactions between NO_x and volatile organic compounds (VOCs), which were
32 substantially reduced during the pandemic. We use satellite measurements of PANs from the Suomi-
33 National Polar-orbiting Partnership (S-NPP) Cross-Track Infrared Sounder (CrIS) in the free troposphere
34 over and surrounding eight of the world's megacities: Mexico City, Beijing, Los Angeles, Tokyo, São
35 Paulo, Delhi, Lagos, and Karachi. Seasonal cycles of PANs are pronounced and the seasonal maxima
36 correspond to seasonal peaks in local photochemistry. Significant changes to PANs in response to
37 COVID-19 occurred over two out of the eight cities: Los Angeles (PANs decreased) and Beijing (PANs
38 increased). Our results indicate that large changes in NO_x may not result in equally significant changes to
39 PANs and the NO_x export potential of megacities.

40 1 Introduction

41 To slow the spread of the 2019 novel coronavirus (COVID-19), urban centers across the globe
42 partially shut down for various amounts of time (Chinazzi et al., 2020; WHO, 2020). While the timing
43 differed for each urban region, a consequence of these bursts of reduced economic activity was a radical
44 decrease in the emissions of many primary air pollutants. Reductions in global and regional particulate
45 matter, nitrogen oxides ($\text{NO}_x = \text{NO} + \text{NO}_2$), carbon dioxide (CO_2), and other trace gasses associated with
46 the COVID-19 pandemic have been documented (Bauwens et al., 2020; Z. Liu et al., n.d.; Miyazaki,
47 Bowman, Sekiya, Jiang, et al., 2020; Miyazaki et al., 2021; Odekanle et al., 2022; Sharma et al., 2020;
48 Shi & Brasseur, 2020; Venter et al., 2020; J. Zhang et al., 2022) Less is understood about changes to
49 secondary pollutants as they respond non-linearly to changes in precursor emissions, and their production
50 and lifetime also depend on environmental conditions (e.g., Stavrou et al., 2021). For example, both
51 increases and decreases in surface ozone (O_3) have been documented in urban areas during the COVID-
52 19 pandemic despite decreases in precursor emissions (e.g., Le et al., 2020; Miyazaki et al., 2021; Qiu et
53 al., 2020; Shi & Brasseur, 2020; Sicard et al., 2020).

54 Peroxyacyl nitrates (PANs) are important photochemically-produced species that are formed
55 alongside O_3 in polluted environments by the oxidation of non-methane volatile organic compounds
56 (NMVOCs) in the presence of NO_x (Fischer et al., 2014; Gaffney et al., 1989; Roberts, 2007; Singh et al.,
57 1986; Singh & Hanst, 1981). PANs are considered to be a sensitive tracer of photochemistry (e.g.,
58 Coggon et al., 2021; Rappenglück et al., 2003). Formation and decomposition of PANs can impact the
59 production of O_3 (e.g. Steiner et al., 2010), the production of PANs acts as an indicator of regional
60 photochemistry (Sillman & West, 2009), and the concentration of PANs can be used to gauge
61 effectiveness of O_3 -control strategies (Gaffney et al., 1989). PANs respond to precursor emissions non-
62 linearly and have been shown to be more sensitive to changes in NMVOCs versus changes in NO_x for

63 many regions of the global atmosphere (Fischer et al., 2014) and in some urban regions (T. Liu et al.,
64 2022).

65 The lifetime of PANs against thermal decomposition is strongly dependent on temperature, where
66 PANs are thermally unstable in the lower troposphere (lifetime on the order of hours at 20°C), but have a
67 lifetime >1 month at temperatures characteristic of the mid-troposphere (Honrath et al., 1996). When
68 transported from polluted continental regions to the remote troposphere, PANs serve as the principal
69 reservoir species for NO_x and can contribute to efficient production of downwind O₃ in NO_x limited
70 conditions (Fischer et al., 2014; Mena-Carrasco et al., 2009). The distribution of O₃ in the remote
71 atmosphere would be substantially different without PAN chemistry (e.g., Jiang et al., 2016). There have
72 been major changes in NO_x and VOC emissions in urban areas in recent decades, elevating the need for
73 continued and extended observations of photochemically-relevant species in urban regions. In situ
74 measurements of PANs have been collected for select urban areas for select seasons (Gaffney et al., 1989;
75 Qiu et al., 2019; G. Zhang et al., 2015a), though observations are generally sparse.

76 Here we present new satellite observations of PANs over eight megacities. We utilize
77 measurements from the Suomi-National Polar-orbiting Partnership (S-NPP) Cross-Track Infrared
78 Sounder (CrIS) and other complimentary satellite and reanalysis datasets to document the seasonal cycles
79 of PANs over select megacities and the response of PANs to COVID-19 induced reductions of precursor
80 concentrations in these locations.

81

82 **2 Materials and Methods**

83 **2.1 CrIS Observations**

84 We use observations of free tropospheric PANs and CO from the CrIS instrument, a nadir
85 viewing Fourier transform spectroradiometer currently flying on the S-NPP satellite. The datasets used
86 here were produced under the NASA Tropospheric Ozone and Precursors from Earth System Sounding
87 (TROPESS) project (Bowman, 2021c, 2021k, 2021o, 2021a, 2021e, 2021i, 2021l, 2021p, 2021d, 2021j,
88 2021b, 2021f, 2021c; Shogrin, 2023). Information on the CrIS PANs retrieval algorithm and validation
89 against aircraft observations can be found in Payne et al. (2022). The validation efforts for the CrIS PANs
90 product suggest a single sounding uncertainty of around 0.08 ppbv that reduces with averaging to an
91 approximate floor of 0.05 ppbv and demonstrates the ability of CrIS to capture variation in the
92 “background” PANs over remote regions (Payne et al., 2022). The CrIS CO algorithm is described in Fu
93 et al. (2016) and validation is presented in Worden et al. (2022). A single sounding uncertainty for CrIS
94 CO retrievals is on the order of 6-10% (Worden et al., 2022) and this is expected to reduce with
95 averaging. Our analysis uses the column average PANs volume mixing ratio (VMR) between 825 and
96 215 hPa. CrIS PANs retrievals have peak sensitivity in the free troposphere (~680 hPa) and the sensitivity
97 decreases rapidly near the surface. At most, CrIS PANs retrievals have 1 degree of freedom for signal
98 (DOF), meaning this product does not include information about the vertical distribution of PANs in the
99 atmosphere. The spectral feature utilized by CrIS for retrieval of PANs is centered at 790 cm⁻¹. This
100 infrared spectral feature appears in the spectra of all PANs at essentially the same frequency, so CrIS
101 measurements include all PAN species (i.e., they include propionyl peroxy nitrate (PPN;
102 CH₃CH₂C(O)OONO₂), methacryloyl peroxy nitrate (MPAN; CH₂C(CH₃)C(O)OONO₂), etc.) in addition
103 to peroxyacetyl nitrate (PAN; CH₃C(O)O₂NO₂). We also use a tropospheric average of CrIS CO between
104 825 hPa and 215 hPa. Our analysis focuses on CrIS PANs over and around 9 megacities utilizing CrIS
105 CO to contextualize seasonal enhancements in PANs.

106

107 PAN observations from nadir-viewing satellites include those from the Tropospheric Emission
108 Spectrometer (TES) (Payne et al., 2014) as well as meteorological sounders namely the Infrared
109 Atmospheric Sounding Interferometer (IASI) (Franco et al., 2018) and CrIS (Payne et al., 2022). Studies
110 observing PAN from space thus far have focused on PAN enhancements associated with fires (Alvarado

111 et al., 2011; Clarisse et al., 2011; Juncosa Calahorrano et al., 2021) and the global distribution of PAN
112 and its role in the long range transport of O₃ (Fischer et al., 2018; Jiang et al., 2016; Payne et al., 2017;
113 Zhu et al., 2015; 2017). Although TES had provided a set of special observations over select megacities
114 (Cady-Pereira et al., 2017; Shogrin et al., 2023), the spatial and temporal coverage of this dataset is
115 somewhat limited. Here, we utilize the more comprehensive spatial and temporal coverage of CrIS to
116 explore the spatiotemporal distribution of PANs over and around megacities.

117 118 **2.2 Ozone Monitoring Instrument (OMI) Observations**

119
120 We use Level 3 NO₂ tropospheric column measurements from NASA Aura-OMI to identify
121 months with anomalously low NO₂ columns associated with COVID in 2020. We use the Quality
122 Assurance for Essential Climate Variables (QA4ECV) NO₂ Level 3 product described in Boersma et al.
123 (2018) as this is the most recently updated data product. OMI NO₂ L3 monthly mean data used in this
124 study is provided on a global 0.125° x 0.125° grid and can be found on the TEMIS database (Boersma et
125 al., 2017b).

126
127 We use Level 3 (L3) HCHO tropospheric column measurements, also from OMI, to contextualize
128 changes in monthly VOC concentrations in megacities during the period of anomalously low tropospheric
129 NO₂. Space-based observations of HCHO are used as an indicator of VOC emissions (De Smedt et al.,
130 2008; Shen et al., 2019). HCHO is also processed using the QA4ECV algorithm consistently with the NO₂
131 data used in this study. HCHO L3 monthly mean data is also provided on a global 0.125° x 0.125° grid
132 and can also be found on the TEMIS database (De Smedt et al., 2017).

133 134 **2.3 Chemical Reanalysis Product**

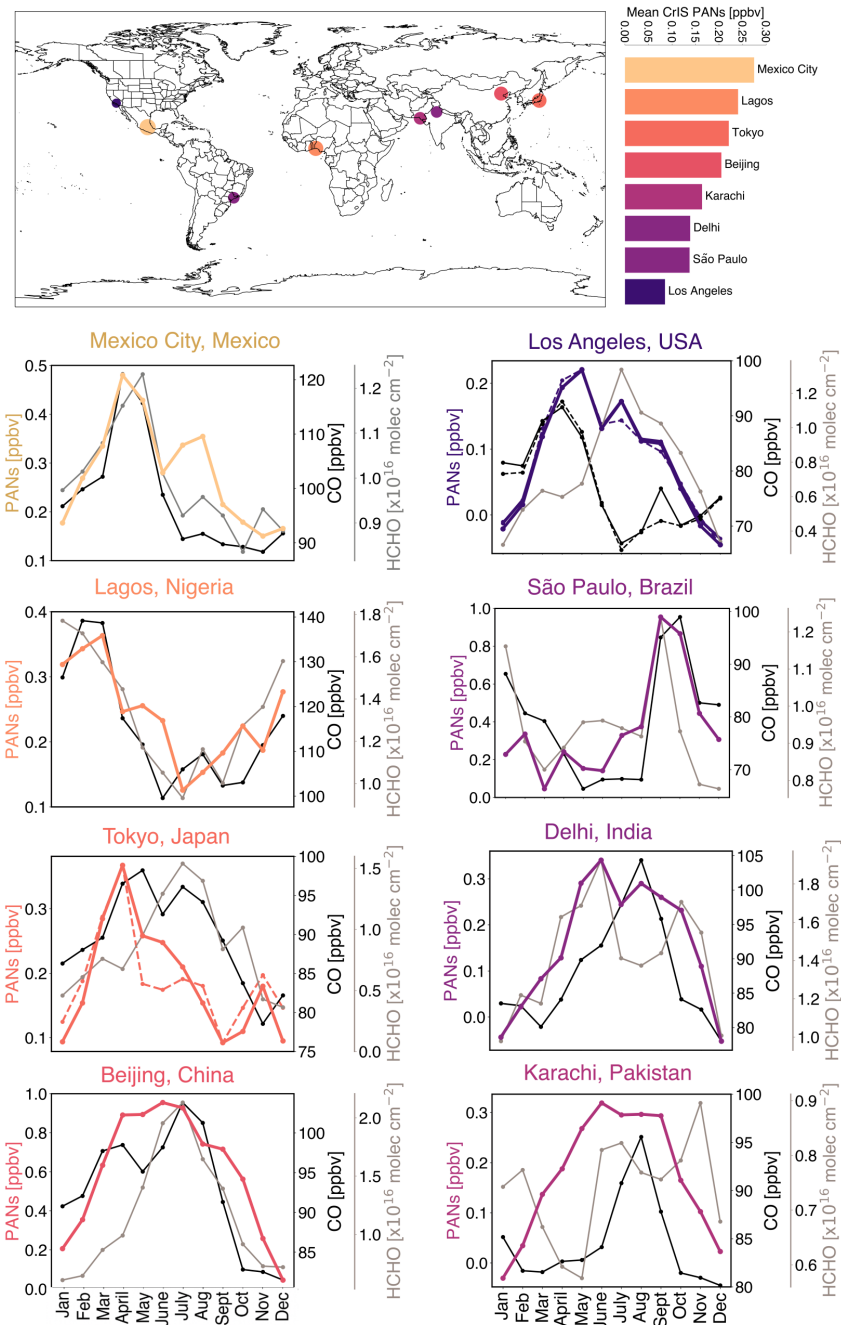
135
136 We use NO_x emission reanalysis data to also place changes to PANs in the context of NO_x emission flux
137 reductions in megacities associated with COVID-19. NO_x emissions are from an assimilation of multi-
138 species satellite observations (O₃, CO, NO₂, HNO₃, and SO₂) in the Tropospheric Chemistry Reanalysis
139 version 2 (TCR-2) framework (Miyazaki et al., 2020; <https://doi.org/10.25966/9qgv-fe81>). NO_x
140 emissions are constrained by tropospheric column NO₂ retrievals from the QA4ECV version 1.1 Level 2
141 products from OMI and Global Ozone Monitoring Experiment 2 (GOME-2) (Boersma et al., 2017a,
142 2017b). A priori emissions are from HTAP version 2 for 2010 (Janssens-Maenhout et al., 2015), Global
143 Fire Emissions Database (GFED) version 4 (Randerson et al., 2018), and the Global Emissions Inventory
144 Activity (GEIA) (Graedel et al., 1993). The reanalysis fields have been evaluated against independent
145 observations on regional and global scales (Miyazaki et al., 2020). NO_x emissions for 2020 used in our
146 analysis are estimated using business as usual (BAU) emissions added to the estimated COVID-19
147 emissions anomaly described in Miyazaki et al. (2021). While the observed NO₂ concentrations are
148 affected by meteorological concentrations, their effect is already taken into account when estimating the
149 NO_x emissions (Miyazaki et al., 2017; 2020)

150
151
152

153

154 **3 Results and discussion**

155 **3.1 Seasonal Cycles of PANs, CO, and HCHO in megacities**



156

157

158 **Figure 1.** Top: Map shows mean detected CrIS PANs for the entire study period. The scale to the right of
 159 the map ranks the cities using the mean PANs. Dot sizing is indicative of abundance of mean PANs.

160 Seasonal cycles of CrIS PANs [ppbv] (color denoted in color bar, dashed denotes median values), CrIS
 161 tropospheric CO [ppbv] (dark grey), and OMI HCHO tropospheric column average [$\times 10^{16}$ molecules cm^{-2}]

162 (lighter grey) for eight megacities. Note: scales vary for each plot. Monthly means include data from
163 January 2016 to May 2021.

164
165 Figure 1 displays the mean seasonal cycles for CrIS PANs, CrIS CO, and OMI HCHO for eight
166 different global megacities from 2016-2021. Figure 1 helps identify periods in the annual cycle with
167 production of PANs and values of PANs above a threshold where CrIS is able to provide quantitative
168 information. For most cities, NO₂ changes from COVID-19 coincide with periods where PANs are above
169 the CrIS detection limit (Section 2.1) and conditions support photochemical production.

170 All but two selected megacities experience a springtime maxima in PANs. The seasonal
171 springtime maximum in PANs is attributed to an increase in photochemical activity at a time when PANs
172 have a relatively long lifetime against thermal decomposition (Brice et al., 1988; Fischer et al., 2014;
173 Penkett & Brice, 1986). Seasonal maxima occur in March, April, and/or May for northern hemisphere
174 megacities (Mexico City, Los Angeles (LA), Tokyo, Delhi, and Lagos), and in September for São Paulo
175 (23.56°S), the beginning of austral spring. Over Lagos (6.52°N) PANs begin increasing towards the end
176 of the calendar year and maximize in March or April. In addition to a springtime maxima, PANs over
177 Beijing (39.92°N) and Karachi (24.86°N) remain elevated through the summer (April-September).
178 Though it has a springtime maxima, Delhi (28.71°N) has a comparably wide seasonal cycle in PANs.
179 Mexico City, LA, and Tokyo also show an additional period of elevated PANs later in the year.

180 PANs over each megacity reflect a combination of sources and meteorological conditions, but the
181 extent of the published literature on air pollutants in each megacity differs widely. Here we focus our
182 discussion on LA, Beijing, and to a more limited extent, Tokyo, Delhi, and Lagos.

183 There is a longstanding effort to attribute and control O₃ and other photochemical pollutants in
184 LA (Langford et al., 2010; Nussbaumer & Cohen, 2020; Pollack et al., 2013; Warneke et al., 2013). CrIS
185 data indicate that the seasonal cycle in PANs over LA is distinct from both HCHO and surface O₃ (not
186 shown); tropospheric column HCHO and surface O₃ have broad maxima extending from April through
187 October and June through October, respectively. Increasing temperatures during the summer decrease the
188 lifetime of PANs due to thermal decomposition and decrease the ratio of free tropospheric PANs to
189 surface O₃. The secondary and tertiary peaks in monthly mean PANs over LA in July and September are
190 driven by wildfire smoke transported into the LA Basin in 2018 and 2020, respectively (Liang et al.,
191 2021). Wildfire impacts in September 2020 also drive the peak in September CO; note the difference
192 between the mean and median as these peaks are not evident in the median (dashed) CO and PANs for
193 these months.

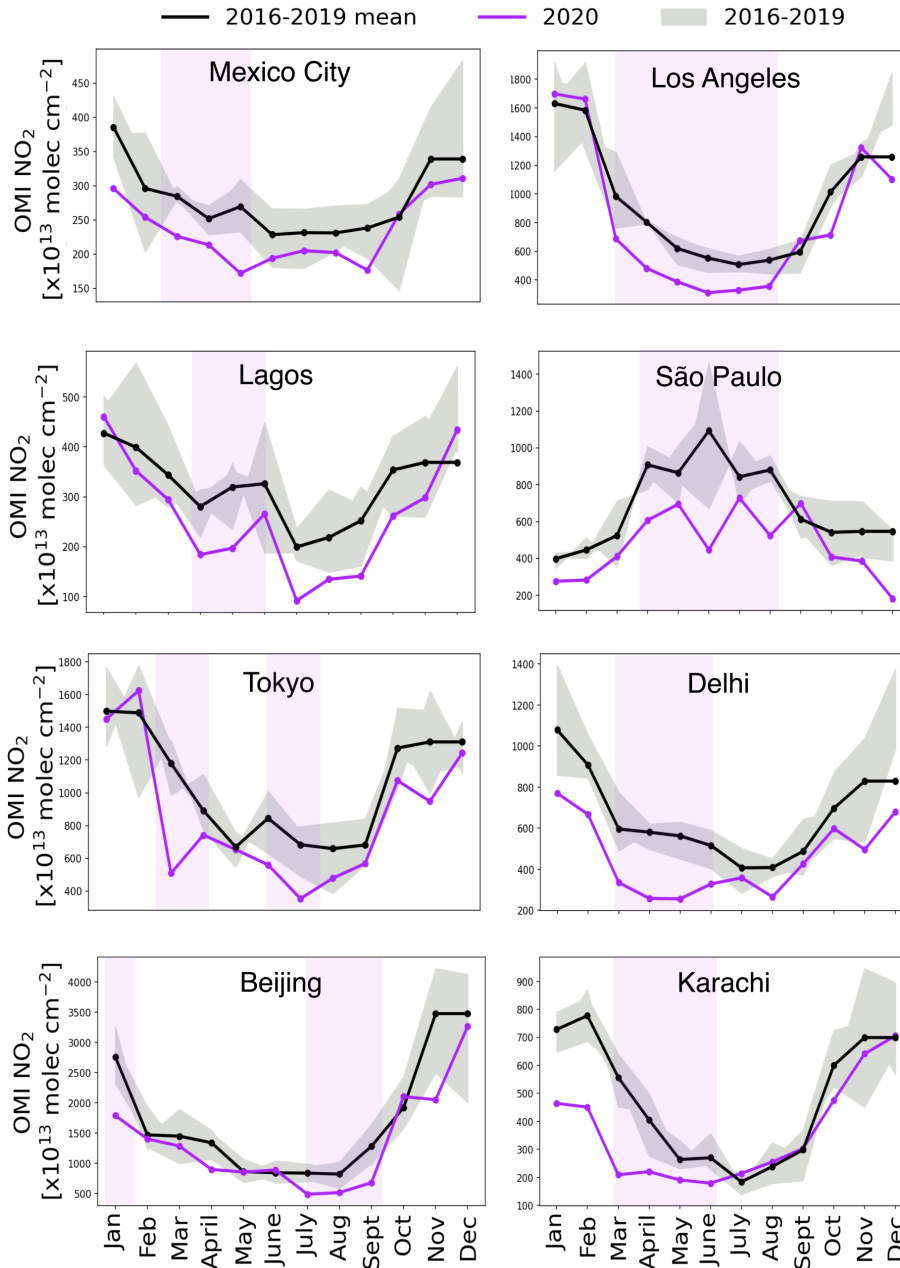
194 Information on PANs within and around Beijing is growing rapidly (e.g., Z. Liu et al., 2010; B.
195 Zhang et al., 2017, 2019). In Beijing, surface O₃ and tropospheric column HCHO have seasonal maxima
196 in summer months (JJA), corresponding to the seasonal maximum in CrIS PANs (Figure 1) and recorded
197 surface observations of PAN and PPN (B. Zhang et al., 2017; G. Zhang et al., 2015b). Ground-level PAN
198 is also elevated during winter haze events in Beijing (Li et al., 2021; Qiu et al., 2019; B. Zhang et al.,
199 2019; G. Zhang et al., 2020). CrIS observes elevated CO over Beijing in March and April, consistent with
200 a seasonal peak in local fire activity in northeast China (Feng et al., 2015; L. Wang et al., 2020; Yin et al.,
201 2019; Zhao et al., 2022).

202 Tokyo has a seasonal spring maximum in photochemical species from both local and distant (*i.e.*,
203 China and Korea) sources of precursors (Lee et al., 2021; Yoshitomi et al., 2011). Delhi has a humid
204 subtropical/semi-arid climate and air pollution is strongly influenced by the Indian monsoon (Gurjar et al.,
205 2016). The monsoon season lasts from July-September and the dry season is considered to be September-
206 June. CrIS observes elevated PANs over Delhi from April to October; on average PANs remain elevated
207 through the monsoon season. Crop residue burning in April-May and October-November can deteriorate
208 air quality in the Delhi metropolitan area (Saxena et al., 2021). These periods correspond with periods of
209 elevated PANs and tropospheric column HCHO. Lagos surface O₃ increases seasonally during the dry
210 season (Abdul Raheem et al., 2009). This is consistent with CrIS observations of PANs and CO, which
211 increase and decrease with the respective dry and wet seasons.

212

213
214

3.2 2020 NO₂ Anomalies



215
216
217
218
219
220
221
222
223

Figure 2. OMI NO₂ tropospheric column monthly means for 9 megacities. The area used for each city is the same area around the urban area of each city used for CrIS selection and this information is provided in Table 1. 2020 is shown in purple. The mean of 2016-2019 is shown in bold black. Months with substantial NO₂ declines in 2020 have been highlighted in purple shading and these time frames are used in the subsequent analysis presented in Figure 3.

Major changes in NO_x emissions and tropospheric NO₂ column abundances have been documented worldwide for different periods of the COVID-19 pandemic (Bauwens et al., 2020; Berman & Ebisu,

224 2020; J. Zhang et al., 2022). For the analysis presented here, we identify periods where 1) the monthly
 225 mean NO₂ column during 2020 was at least 15% below the corresponding monthly mean for 2016-2019
 226 (black line in Figure 2), and 2) the monthly mean PANs mixing ratio are at least 0.05 ppbv (Figure 1). We
 227 only consider times in the seasonal cycle where mixing ratios of PANs are at least 0.05 ppbv because this
 228 corresponds with the uncertainty discussed in Section 2.1 and Payne et al. (2022). The months that meet
 229 these criteria are highlighted by the light purple shading in Figure 2. The 2020 monthly mean NO₂
 230 column density associated with these shaded periods is at least 15% less than the mean of the
 231 corresponding months for the period 2016-2019. Periods of lower observed NO₂ often do not exactly
 232 coincide with the COVID-19 government-enforced lockdowns, as reduced traffic was often observed
 233 prior to government-imposed stay-at-home orders.

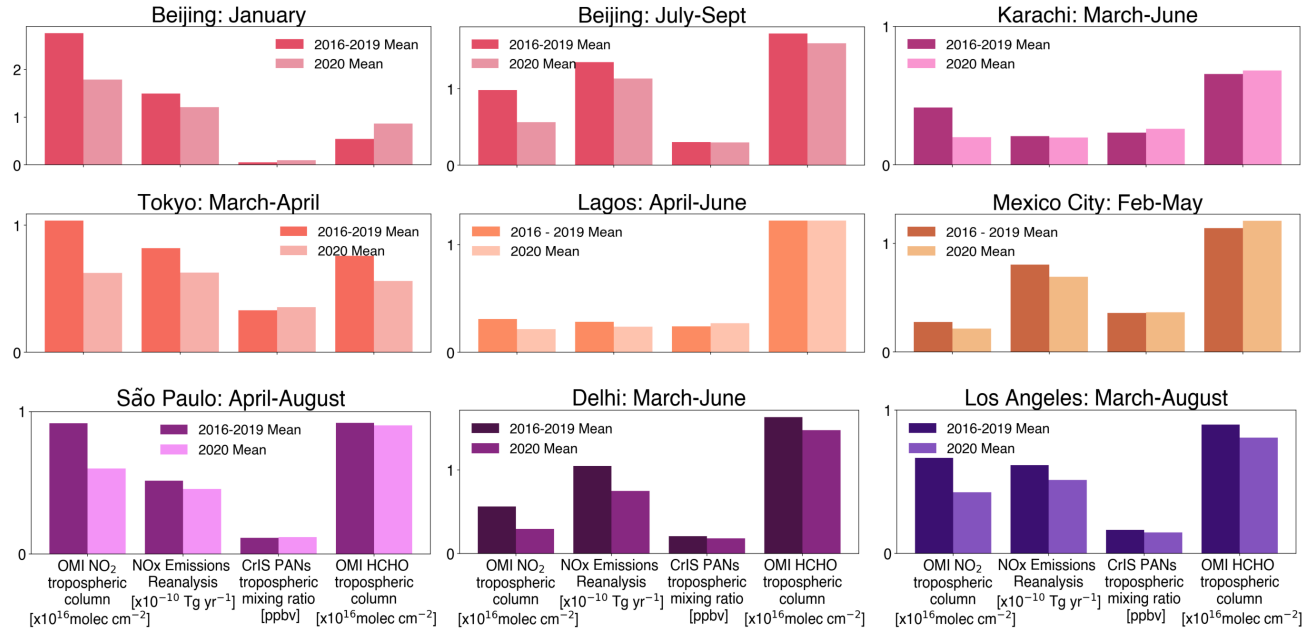
234
 235 **Table 1.** Changes to Chemical Species during Respective Time Periods.
 236

City	Monthly mean time period	NO ₂ change (%)	NO _x change (%)	HCHO change (%)	PANs change (%)	P-value
Mexico City	February-May	-22%	-14%	5.6%	1.8%	0.45
Beijing	January	-35%	-19%	59%	80%	0.03
Beijing	July-September	-40%	-16%	-7.6%	-1.9%	0.31
Tokyo	March-April	-40%	-23%	-26%	6.9%	0.11
Tokyo	June-July	-40%	-15%	-43%	-0.9%	0.44
Los Angeles	March-August	-36%	-17%	-10%	-11%	0.06
São Paulo	April-August	-35%	-11%	-1.7%	3.7%	0.33
Delhi	March-June	-48%	-28%	-9.6%	-20%	0.33
Lagos	April-June	-35%	-16%	-0.08%	11%	0.33
Karachi	March-June	-52%	-5%	3.6%	12%	0.14

237
 238 **Table 1.** Periods of significant NO₂ decline based on tropospheric column OMI NO₂ monthly means
 239 shown in Figure 2. Percent change represents the change in 2020 values relative to the mean of 2016-
 240 2019 for the respective time periods. Percent change in PANs were calculated using daily means during
 241 the months of NO₂ anomaly. P-values are from Mann-Whitney u test. A negative percent change signifies
 242 a decline in 2020 relative to the same months in prior years; likewise, positive percent changes signify an
 243 increase.
 244
 245
 246
 247
 248
 249
 250
 251
 252
 253
 254

255

3.3 Impacts of COVID-19 NO_x reductions on PANs over megacities



256

257

258

259

260

261

262

263

264

265

266

267

268

269

270

271

272

273

274

275

276

277

278

279

280

281

282

283

284

285

286

Figure 3. Bar charts comparing monthly means for specified months of OMI NO₂ tropospheric columns [$\times 10^{16}$ molecules cm^{-2}], NO_x emissions from the Tropospheric Chemical Reanalysis [$\times 10^{-10}$ Tg yr^{-1}], CrIS free troposphere PANs [ppbv], and OMI HCHO tropospheric columns [$\times 10^{16}$ molecules cm^{-2}] for each megacity. Means of monthly means for specified periods in 2020 (shown in Figure 2 and listed in Table 1) are plotted in the lighter colors and means of 2016-2019 are plotted in the darker colors. We performed a Mann-Whitney u-test to test the significance of changes to PANs during the respective time periods of COVID-19 NO₂ perturbations listed in Table 1; 2020 was compared to the same time period from 2016-2019. We set our alpha at 0.1, so p values < 0.1 are considered significant and receive more discussion.

Figure 3 shows that while there were large decreases in NO₂ declines at some point in 2020, this did not yield a similarly large change in free tropospheric PANs for each region. Most megacities surveyed did not experience significant change in PANs at the 90% confidence level, except for LA, which experienced a significant decline, and Beijing in winter, which experienced a significant increase. We expect that PANs (and the sensitivity of CrIS) would also respond to other environmental factors including temperature; we analyze two possible environmental indicators: 2 meter air temperature and 500 hPa air temperature changes between the two respective periods over each of the megacities using MERRA-2 Reanalysis monthly mean product (Global Modeling and Assimilation Office (GMAO), 2015; DOI:10.5067/AP1B0BA5PD2K). We find no significant change in mean temperature at either pressure level between 2020 and corresponding months during the prior 4 years. Thus temperature was likely not a significant factor driving anomalies in PANs during the extended periods of NO_x perturbations highlighted in Figure 2. PANs have been used to gauge effectiveness of O₃-control strategies (*e.g.*, Gaffney et al., 1989). The tropospheric column ratios of HCHO to NO₂ have been used as a qualitative indicator of NO_x sensitive versus NO_x saturated (VOC-limited) regimes (*e.g.*, Jin et al., 2017; Martin et al., 2004; Sourì et al., 2023). Threshold values vary by location (Sourì et al., 2020), but higher (lower) ratios indicate NO_x-sensitive (saturated) conditions. Reductions in NO_x during the pandemic were substantial enough to shift the photochemical regime in some areas, *i.e.*, from NO_x-saturated to a transition zone or from a transition zone to NO_x-sensitive conditions (Peralta et al., 2021). The SI contains a version of Table 1 that also includes tropospheric column HCHO:NO₂ ratios over each city. We did not

287 identify a consistent relationship between this ratio and the sensitivity of PAN to COVID induced-
288 changes to NO_x.

289 PANs decreased significantly over LA during COVID-19 NO_x emission reductions, and this
290 coincided with decreases in surface O₃ (Connerton et al., 2020; Schroeder et al., 2022). The underlying
291 photochemical environment of LA has been transitioning from a VOC-limited regime to a NO_x-limited
292 regime (Lee et al., 2021; Schroeder et al., 2022); spring 2020 was the first NO_x-limited year (Schroeder et
293 al., 2022). PAN abundances at the ground have decreased much more rapidly than O₃ in response to
294 emission controls in the LA Basin (Pollack et al., 2013). The CrIS data suggest that PAN would continue
295 to respond to NO_x emission reductions in this city.

296 PANs did not show marked changes over Mexico City, São Paulo or Tokyo despite major NO_x
297 perturbations. O₃ over Tokyo also did not significantly change with COVID-19 lockdown measures; this
298 has been attributed to a shift in the underlying photochemical regime from VOC-limited towards the
299 transition zone where O₃ production is expected to be equally sensitive to changes in both NO_x and VOCs
300 (Damiani et al., 2022; Ito et al., 2021; Q. Wang & Li, 2021). O₃ in Mexico City was also statistically
301 indistinguishable during periods of substantial precursor reduction in 2020 from that of other years
302 (Peralta et al., 2021). São Paulo experienced an increase in O₃ in April and May, but largely in areas most
303 seriously impacted by vehicle emissions (Alvim et al., 2023).

304 The largest and only significant increase in free tropospheric PANs on a monthly mean scale in
305 our analysis occurred over Beijing in January (80%, $p = 0.03$), coincident with the lowest average HCHO:
306 NO₂ ratio of all cities included here. Qiu et al. (2020) reported a threefold increase in ground-level PAN
307 in urban Beijing during this first lockdown period, connected to enhanced local photochemistry and
308 abnormal meteorological conditions, including anomalous wind convergence under higher temperatures.
309 We find a similar change in free tropospheric PANs over Beijing, where mean CrIS PANs are 2.4 times
310 higher during the same lockdown period. Beijing had a second period of NO₂ decline in July and August
311 2020, which was associated with an insignificant change in PANs (-1.96%, $p = 0.31$). Stavrakou et al.
312 (2021) also investigated the impact of COVID-19 on PAN over China.

313

314 **5 Conclusions**

315 We use CrIS data from 2016-2021 to identify the seasonality of PANs over 8 megacities, and identify
316 time periods with elevated PANs. This is the first detailed analysis of satellite observations of PANs over
317 multiple megacities. We use this to inform our analysis in diagnosing the impact of NO₂ declines related
318 to the COVID-19 pandemic on PANs in these locations.

319

320

321 1. There are pronounced seasonal cycles in PANs over each megacity. Monthly mean PANs peak in
322 the spring or summer (Beijing and Karachi), aligning with respective seasonal maximums in
323 photochemical activity. Wildfire smoke can occasionally enhance monthly mean PANs.

324

325

326 2. Despite large changes in tropospheric NO₂ columns associated with the COVID-19 pandemic, we
327 only identify two megacities over which PANs changed significantly: Beijing and LA. The
328 relative response of PANs in these locations was smaller than the changes in NO₂. The response
329 of PANs to a major change in precursor emissions is highly non-linear.

330

331

332 3. Sensitivity of free tropospheric PANs to the abundance of precursors appears to be seasonally
333 dependent in Beijing and Tokyo. PANs over Beijing and Tokyo are likely more sensitive to NO_x
334 reductions in winter and spring respectively.

335
336
337
338
339
340
341

4. Based on this survey of megacities, relatively large perturbations in NO_x may not result in significant declines in NO_x export potential of megacities in all seasons. Thus satellite observations of PANs may be an additional useful diagnostic in predicting the complex response of O₃ to NO_x reductions in downwind regions. Next steps should focus on identifying the response of PAN downwind of megacities to COVID-19 NO_x reductions.

342 **Acknowledgments**

343 This work is funded under NASA award no. 80NSSC20K0947. Part of this work was carried out
344 at the Jet Propulsion Laboratory, California Institute of Technology, under a contract with the
345 National Aeronautics and Space Administration (80NM0018D0004). We thank Isabelle De
346 Smedt and Folkert Boersma for collaborating on the proposal that led to this work and for
347 answering questions regarding the OMI data.

348

349 **Open Research**

350 The Summary and Standard Product of CrIS PANs megacity Special Collection data for each
351 megacity used in this study are available online through the Goddard Earth Sciences Data and
352 Information services Center (NASA GES DISC) (Bowman, 2021c, 2021k, 2021g, 2021o, 2021a,
353 2021e, 2021m, 2021i, 2021l, 2021h, 2021p, 2021d, 2021n, 2021j, 2021b, 2021f, 2021c). Megacity
354 datasets for Lagos and São Paulo can be found at <https://doi.org/10.5061/dryad.wpzgmsbtk> and
355 eventually on the NASA GES DISC. OMI NO₂ and HCHO data were obtained from
356 <https://www.temis.nl/airpollution/no2.php> and <https://h2co.aeronomie.be/> (last access: August 2021),
357 (Boersma et al., 2017b; De Smedt et al., 2017).

358
359

360

361

362

363

364

365

366

367

368

369 **References**

- 370 Abdul Raheem, A. M. O., Adekola, F. A., & Obioh, I. O. (2009). The Seasonal Variation of the
371 Concentrations of Ozone, Sulfur Dioxide, and Nitrogen Oxides in Two Nigerian Cities.
372 *Environmental Modeling & Assessment*, *14*(4), 497–509. [https://doi.org/10.1007/s10666-](https://doi.org/10.1007/s10666-008-9142-x)
373 [008-9142-x](https://doi.org/10.1007/s10666-008-9142-x)
- 374 Alvarado, M. J., Cady-Pereira, K. E., Xiao, Y., Millet, D. B., & Payne, V. H. (2011). Emission
375 Ratios for Ammonia and Formic Acid and Observations of Peroxy Acetyl Nitrate (PAN)
376 and Ethylene in Biomass Burning Smoke as Seen by the Tropospheric Emission
377 Spectrometer (TES). *Atmosphere*, *2*(4), 633–654. <https://doi.org/10.3390/atmos2040633>
- 378 Alvim, D. S., Herdies, D. L., Corrêa, S. M., Basso, L. S., Khalid, B., Silva, G. F. P., Oyerinde,
379 G., De Carvalho, N. A., Coelho, S. M. S. D. C., & Figueroa, S. N. (2023). COVID-19
380 Pandemic: Impacts on Air Quality during Partial Lockdown in the Metropolitan Area of
381 São Paulo. *Remote Sensing*, *15*(5), 1262. <https://doi.org/10.3390/rs15051262>
- 382 Bauwens, M., Compernelle, S., Stavrou, T., Müller, J. -F., Gent, J., Eskes, H., Levelt, P. F., A,
383 R., Veefkind, J. P., Vlietinck, J., Yu, H., & Zehner, C. (2020). Impact of Coronavirus
384 Outbreak on NO₂ Pollution Assessed Using TROPOMI and OMI Observations.
385 *Geophysical Research Letters*, *47*(11). <https://doi.org/10.1029/2020GL087978>
- 386 Berman, J. D., & Ebisu, K. (2020). Changes in U.S. air pollution during the COVID-19
387 pandemic. *Science of The Total Environment*, *739*, 139864.
388 <https://doi.org/10.1016/j.scitotenv.2020.139864>
- 389 Boersma, K. F., Eskes, H. J., Richter, A., De Smedt, I., Lorente, A., Beirle, S., van Geffen, J. H.
390 G. M., Zara, M., Peters, E., Van Roozendaal, M., Wagner, T., Maasakkers, J. D., van der
391 A, R. J., Nightingale, J., De Rudder, A., Irie, H., Pinardi, G., Lambert, J.-C., &

- 392 Compernelle, S. C. (2018). Improving algorithms and uncertainty estimates for satellite
393 NO₂ retrievals: Results from the quality assurance for the
394 essential climate variables (QA4ECV) project. *Atmospheric Measurement Techniques*,
395 *11*(12), 6651–6678. <https://doi.org/10.5194/amt-11-6651-2018>
- 396 Boersma, K. F., Eskes, H., Richter, A., De Smedt, I., Lorente, A., Beirle, S., van Geffen, J. H. G.
397 M., Peters, E., Van Roozendaal, M., & Wagner, T. (2017a). *QA4ECV NO₂ tropospheric*
398 *and stratospheric vertical column data from GOME-2A (Version 1.1) [Data set]*. Royal
399 Netherlands Meteorological Institute (KNMI). [http://doi.org/10.21944/qa4ecv-no2-](http://doi.org/10.21944/qa4ecv-no2-gome2a-v1.1)
400 [gome2a-v1.1](http://doi.org/10.21944/qa4ecv-no2-gome2a-v1.1)
- 401 Boersma, K. F., Eskes, H., Richter, A., De Smedt, I., Lorente, A., Beirle, S., van Geffen, J. H. G.
402 M., Peters, E., Van Roozendaal, M., & Wagner, T. (2017b). *QA4ECV NO₂ tropospheric*
403 *and stratospheric vertical column data from OMI (Version 1.1) [Data set]*. Royal
404 Netherlands Meteorological Institute (KNMI). [http://doi.org/10.21944/qa4ecv-no2-omi-](http://doi.org/10.21944/qa4ecv-no2-omi-v1.1)
405 [v1.1](http://doi.org/10.21944/qa4ecv-no2-omi-v1.1)
- 406 Bowman, K. W. (2021a). *TROPESS CrIS-SNPP L2 Peroxyacetyl Nitrate for Beijing* (Standard
407 Product V1) [dataset]. Goddard Earth Sciences Data and Information Services Center
408 (GES DISC). <https://doi.org/10.5067/IUJHNI1MM1QA>
- 409 Bowman, K. W. (2021b). *TROPESS CrIS-SNPP L2 Peroxyacetyl Nitrate for Beijing* (Summary
410 Product V1) [dataset]. Goddard Earth Sciences Data and Information Services Center
411 (GES DISC). <https://doi.org/10.5067/GBMBES47TUOI>
- 412 Bowman, K. W. (2021c). *TROPESS CrIS-SNPP L2 Peroxyacetyl Nitrate for Delhi* (Standard
413 Product V1) [dataset]. Goddard Earth Sciences Data and Information Services Center
414 (GES DISC). <https://doi.org/10.5067/NILL9KD1K78G>

- 415 Bowman, K. W. (2021d). *TROPESS CrIS-SNPP L2 Peroxyacetyl Nitrate for Delhi* (Summary
416 Product V1) [dataset]. Goddard Earth Sciences Data and Information Services Center
417 (GES DISC). <https://doi.org/10.5067/IHXG5JVO98VC>
- 418 Bowman, K. W. (2021e). *TROPESS CrIS-SNPP L2 Peroxyacetyl Nitrate for Karachi* (Standard
419 Product V1) [dataset]. Goddard Earth Sciences Data and Information Services Center
420 (GES DISC). <https://doi.org/10.5067/3AKYF8OS8DHK>
- 421 Bowman, K. W. (2021f). *TROPESS CrIS-SNPP L2 Peroxyacetyl Nitrate for Karachi* (Summary
422 Product V1) [dataset]. Goddard Earth Sciences Data and Information Services Center
423 (GES DISC). <https://doi.org/OHZ38O337SMK>
- 424 Bowman, K. W. (2021g). *TROPESS CrIS-SNPP L2 Peroxyacetyl Nitrate for Lagos* (Standard
425 Product, V1) [dataset]. Goddard Earth Sciences Data and Information Services Center
426 (GES DISC). <https://doi.org/10.5067/4UH0WF2HOHHB>
- 427 Bowman, K. W. (2021h). *TROPESS CrIS-SNPP L2 Peroxyacetyl Nitrate for Lagos* (Summary
428 Product V1) [dataset]. Goddard Earth Sciences Data and Information Services Center
429 (GES DISC). <https://doi.org/10.5067/G2FKY92PRSF5>,
- 430 Bowman, K. W. (2021i). *TROPESS CrIS-SNPP L2 Peroxyacetyl Nitrate for Los Angeles*
431 (Standard Product V1) [dataset]. Goddard Earth Sciences Data and Information Services
432 Center (GES DISC). <https://doi.org/10.5067/0QPQFIXDET1X>
- 433 Bowman, K. W. (2021j). *TROPESS CrIS-SNPP L2 Peroxyacetyl Nitrate for Los Angeles*
434 (Summary Product V1) [dataset]. Goddard Earth Sciences Data and Information Services
435 Center (GES DISC). <https://doi.org/10.5067/H66DGC3ICJMQ>

- 436 Bowman, K. W. (2021k). *TROPESS CrIS-SNPP L2 Peroxyacetyl Nitrate for Mexico City*
437 (Standard Product V1) [dataset]. Goddard Earth Sciences Data and Information Services
438 Center (GES DISC). <https://doi.org/10.5067/PECEC1AZ5R1J>
- 439 Bowman, K. W. (2021l). *TROPESS CrIS-SNPP L2 Peroxyacetyl Nitrate for Mexico City*
440 (Summary Product V1) [dataset]. Goddard Earth Sciences Data and Information Services
441 Center (GES DISC). <https://doi.org/10.5067/YTO4AV07QQOW>
- 442 Bowman, K. W. (2021m). *TROPESS CrIS-SNPP L2 Peroxyacetyl Nitrate for São Paulo*
443 (Standard Product V1) [dataset]. Goddard Earth Sciences Data and Information Services
444 Center (GES DISC). <https://doi.org/10.5067/SQVOPBQTHU10>
- 445 Bowman, K. W. (2021n). *TROPESS CrIS-SNPP L2 Peroxyacetyl Nitrate for São Paulo*
446 (Summary Product V1) [dataset]. Goddard Earth Sciences Data and Information Services
447 Center (GES DISC). <https://doi.org/10.5067/AA26EWZUNMDK>
- 448 Bowman, K. W. (2021o). *TROPESS CrIS-SNPP L2 Peroxyacetyl Nitrate for Tokyo* (Standard
449 Product V1) [dataset]. Goddard Earth Sciences Data and Information Services Center
450 (GES DISC). <https://doi.org/10.5067/4UH0WF2HOHHB>
- 451 Bowman, K. W. (2021p). *TROPESS CrIS-SNPP L2 Peroxyacetyl Nitrate for Tokyo* (Summary
452 Product V1) [dataset]. Goddard Earth Sciences Data and Information Services Center
453 (GES DISC). <https://doi.org/10.5067/RAD13QSZ61JY>
- 454 Brice, K. A., Bottenheim, J. W., Anlauf, K. G., & Wiebe, H. A. (1988). Long-term
455 measurements of atmospheric peroxyacetyl nitrate (PAN) at rural sites in Ontario and
456 Nova Scotia; seasonal variations and long-range transport. *Tellus B*, 40B(5), 408–425.
457 <https://doi.org/10.1111/j.1600-0889.1988.tb00113.x>

- 458 Cady-Pereira, K. E., Payne, V. H., Neu, J. L., Bowman, K. W., Miyazaki, K., Marais, E. A.,
459 Kulawik, S., Tzompa-Sosa, Z. A., & Hegarty, J. D. (2017). Seasonal and spatial changes
460 in trace gases over megacities from Aura TES observations: Two case studies.
461 *Atmospheric Chemistry and Physics*, 17(15), 9379–9398. [https://doi.org/10.5194/acp-17-](https://doi.org/10.5194/acp-17-9379-2017)
462 9379-2017
- 463 Chinazzi, M., Davis, J. T., Ajelli, M., Gioannini, C., Litvinova, M., Merler, S., Pastore y Piontti,
464 A., Mu, K., Rossi, L., Sun, K., Viboud, C., Xiong, X., Yu, H., Halloran, M. E., Longini,
465 I. M., & Vespignani, A. (2020). The effect of travel restrictions on the spread of the 2019
466 novel coronavirus (COVID-19) outbreak. *Science*, 368(6489), 395–400.
467 <https://doi.org/10.1126/science.aba9757>
- 468 Clarisse, L., R'Honi, Y., Coheur, P.-F., Hurtmans, D., & Clerbaux, C. (2011). Thermal infrared
469 nadir observations of 24 atmospheric gases: TRACE GAS OBSERVATIONS FROM
470 IASI. *Geophysical Research Letters*, 38(10), n/a-n/a.
471 <https://doi.org/10.1029/2011GL047271>
- 472 Coggon, M. M., Gkatzelis, G. I., McDonald, B. C., Gilman, J. B., Schwantes, R. H., Abuhassan,
473 N., Aikin, K. C., Arend, M. F., Berkoff, T. A., Brown, S. S., Campos, T. L., Dickerson,
474 R. R., Gronoff, G., Hurley, J. F., Isaacman-VanWertz, G., Koss, A. R., Li, M., McKeen,
475 S. A., Moshary, F., ... Warneke, C. (2021). Volatile chemical product emissions enhance
476 ozone and modulate urban chemistry. *Proceedings of the National Academy of Sciences*,
477 118(32), e2026653118. <https://doi.org/10.1073/pnas.2026653118>
- 478 Connerton, P., Vicente de Assunção, J., Maura de Miranda, R., Dorothée Slovic, A., José Pérez-
479 Martínez, P., & Ribeiro, H. (2020). Air Quality during COVID-19 in Four Megacities:

- 480 Lessons and Challenges for Public Health. *International Journal of Environmental*
481 *Research and Public Health*, 17(14), 5067. <https://doi.org/10.3390/ijerph17145067>
- 482 Damiani, A., Irie, H., Belikov, D. A., Kaizuka, S., Hoque, H. M. S., & Cordero, R. R. (2022).
483 Peculiar COVID-19 effects in the Greater Tokyo Area revealed by spatiotemporal
484 variabilities of tropospheric gases and light-absorbing aerosols. *Atmospheric Chemistry*
485 *and Physics*, 22(18), 12705–12726. <https://doi.org/10.5194/acp-22-12705-2022>
- 486 De Smedt, I., Müller, J.-F., Stavrou, T., van der A, R., Eskes, H., & Van Roozendaal, M.
487 (2008). Twelve years of global observations of formaldehyde in the troposphere using
488 GOME and SCIAMACHY sensors. *Atmospheric Chemistry and Physics*, 8(16), 4947–
489 4963. <https://doi.org/10.5194/acp-8-4947-2008>
- 490 De Smedt, I., Yu, H., Richter, A., Beirle, S., Eskes, H., Boersma, F., Van Roozendaal, M., van
491 Geffen, J. H. G. M., Lorente, A., & Peters, E. (2017). *QA4ECV HCHO tropospheric*
492 *column data from OMI (Version 1.1) [L3 Monthly Means]*. Royal Belgian Institute for
493 Space Aeronomy. <http://doi.org/10.18758/71021031>
- 494 Feng, X., Li, Q., Zhu, Y., Hou, J., Jin, L., & Wang, J. (2015). Artificial neural networks
495 forecasting of PM_{2.5} pollution using air mass trajectory based geographic model and
496 wavelet transformation. *Atmospheric Environment*, 107, 118–128.
497 <https://doi.org/10.1016/j.atmosenv.2015.02.030>
- 498 Fischer, E. V., Jacob, D. J., Yantosca, R. M., Sulprizio, M. P., Millet, D. B., Mao, J., Paulot, F.,
499 Singh, H. B., Roiger, A., Ries, L., Talbot, R. W., Dzepina, K., & Pandey Deolal, S.
500 (2014). Atmospheric peroxyacetyl nitrate (PAN): A global budget and source attribution.
501 *Atmospheric Chemistry and Physics*, 14(5), 2679–2698. [https://doi.org/10.5194/acp-14-](https://doi.org/10.5194/acp-14-2679-2014)
502 2679-2014

- 503 Fischer, E. V., Zhu, L., Payne, V. H., Worden, J. R., Jiang, Z., Kulawik, S. S., Brey, S.,
504 Hecobian, A., Gombos, D., Cady-Pereira, K., & Flocke, F. (2018). Using TES retrievals
505 to investigate PAN in North American biomass burning plumes. *Atmospheric Chemistry
506 and Physics*, 18(8), 5639–5653. <https://doi.org/10.5194/acp-18-5639-2018>
- 507 Franco, B., Clarisse, L., Stavrou, T., Müller, J. -F, Van Damme, M., Whitburn, S., Hadji-
508 Lazaro, J., Hurtmans, D., Taraborrelli, D., Clerbaux, C., & Coheur, P. -F. (2018). A
509 General Framework for Global Retrievals of Trace Gases From IASI: Application to
510 Methanol, Formic Acid, and PAN. *Journal of Geophysical Research: Atmospheres*,
511 123(24). <https://doi.org/10.1029/2018JD029633>
- 512 Fu, D., Bowman, K. W., Worden, H. M., Natraj, V., Worden, J. R., Yu, S., Veeffkind, P., Aben,
513 I., Landgraf, J., Strow, L., & Han, Y. (2016). High-resolution tropospheric carbon
514 monoxide profiles retrieved from CrIS and TROPOMI. *Atmospheric Measurement
515 Techniques*, 9(6), 2567–2579. <https://doi.org/10.5194/amt-9-2567-2016>
- 516 Gaffney, J. S., Marley, N. A., & Prestbo, E. W. (1989). Peroxyacyl Nitrates (PANs): Their
517 Physical and Chemical Properties. In O. Hutzinger (Ed.), *Air Pollution: Vol. 4 / 4B* (pp.
518 1–38). Springer Berlin Heidelberg. https://doi.org/10.1007/978-3-540-46113-5_1
- 519 Global Modeling and Assimilation Office (GMAO). (2015). *MERRA-2 tavgM_2d_slv_Nx:*
520 *2d, Monthly mean, Time-Averaged, Single-Level, Assimilation, Single-Level Diagnostics*
521 *V5.12.4*. Greenbelt, MD, USA, Goddard Earth Sciences Data and Information Services
522 Center (GES DISC). 10.5067/AP1B0BA5PD2K
- 523 Graedel, T. E., Bates, T. S., Bouwman, A. F., Cunnold, D., Dignon, J., Fung, I., Jacob, D. J.,
524 Lamb, B. K., Logan, J. A., Marland, G., Middleton, P., Pacyna, J. M., Placet, M., &

- 525 Veldt, C. (1993). A compilation of inventories of emissions to the atmosphere. *Global*
526 *Biogeochemical Cycles*, 7(1), 1–26. <https://doi.org/10.1029/92GB02793>
- 527 Gurjar, B. R., Ravindra, K., & Nagpure, A. S. (2016). Air pollution trends over Indian megacities
528 and their local-to-global implications. *Atmospheric Environment*, 142, 475–495.
529 <https://doi.org/10.1016/j.atmosenv.2016.06.030>
- 530 Honrath, R. E., Hamlin, A. J., & Merrill, J. T. (1996). Transport of ozone precursors from the
531 Arctic troposphere to the North Atlantic region. *Journal of Geophysical Research*,
532 101(D22), 29335–29351. <https://doi.org/10.1029/95JD02673>
- 533 Ito, A., Wakamatsu, S., Morikawa, T., & Kobayashi, S. (2021). 30 Years of Air Quality Trends
534 in Japan. *Atmosphere*, 12(8), 1072. <https://doi.org/10.3390/atmos12081072>
- 535 Janssens-Maenhout, G., Crippa, M., Guizzardi, D., Dentener, F., Muntean, M., Pouliot, G.,
536 Keating, T., Zhang, Q., Kurokawa, J., Wankmüller, R., Denier van der Gon, H., Kuenen,
537 J. J. P., Klimont, Z., Frost, G., Darras, S., Koffi, B., & Li, M. (2015). HTAP_v2.2: A
538 mosaic of regional and global emission grid maps for 2008 and 2010 to study
539 hemispheric transport of air pollution. *Atmospheric Chemistry and Physics*, 15(19),
540 11411–11432. <https://doi.org/10.5194/acp-15-11411-2015>
- 541 Jiang, Z., Worden, J. R., Payne, V. H., Zhu, L., Fischer, E., Walker, T., & Jones, D. B. A. (2016).
542 Ozone export from East Asia: The role of PAN. *Journal of Geophysical Research:*
543 *Atmospheres*, 121(11), 6555–6563. <https://doi.org/10.1002/2016JD024952>
- 544 Jin, X., Fiore, A. M., Murray, L. T., Valin, L. C., Lamsal, L. N., Duncan, B., Folkert Boersma,
545 K., De Smedt, I., Abad, G. G., Chance, K., & Tonnesen, G. S. (2017). Evaluating a
546 Space-Based Indicator of Surface Ozone-NO_x-VOC Sensitivity Over Midlatitude
547 Source Regions and Application to Decadal Trends: Space-Based Indicator of O₃

- 548 Sensitivity. *Journal of Geophysical Research: Atmospheres*, 122(19), 10,439-10,461.
549 <https://doi.org/10.1002/2017JD026720>
- 550 Juncosa Calahorrano, J. F., Payne, V. H., Kulawik, S., Ford, B., Flocke, F., Campos, T., &
551 Fischer, E. V. (2021). Evolution of Acyl Peroxynitrates (PANs) in Wildfire Smoke
552 Plumes Detected by the Cross-Track Infrared Sounder (CrIS) Over the Western U.S.
553 During Summer 2018. *Geophysical Research Letters*, 48(23).
554 <https://doi.org/10.1029/2021GL093405>
- 555 Langford, A. O., Senff, C. J., Alvarez, R. J., Banta, R. M., & Hardesty, R. M. (2010). Long-
556 range transport of ozone from the Los Angeles Basin: A case study: LONG-RANGE
557 TRANSPORT OF OZONE. *Geophysical Research Letters*, 37(6), n/a-n/a.
558 <https://doi.org/10.1029/2010GL042507>
- 559 Le, T., Wang, Y., Liu, L., Yang, J., Yung, Y. L., Li, G., & Seinfeld, J. H. (2020). Unexpected air
560 pollution with marked emission reductions during the COVID-19 outbreak in China.
561 *Science*, 369(6504), 702–706. <https://doi.org/10.1126/science.abb7431>
- 562 Lee, H.-J., Chang, L.-S., Jaffe, D. A., Bak, J., Liu, X., Abad, G. G., Jo, H.-Y., Jo, Y.-J., Lee, J.-
563 B., & Kim, C.-H. (2021). Ozone Continues to Increase in East Asia Despite Decreasing
564 NO₂: Causes and Abatements. *Remote Sensing*, 13(11), 2177.
565 <https://doi.org/10.3390/rs13112177>
- 566 Li, K., Jacob, D. J., Liao, H., Qiu, Y., Shen, L., Zhai, S., Bates, K. H., Sulprizio, M. P., Song, S.,
567 Lu, X., Zhang, Q., Zheng, B., Zhang, Y., Zhang, J., Lee, H. C., & Kuk, S. K. (2021).
568 Ozone pollution in the North China Plain spreading into the late-winter haze season.
569 *Proceedings of the National Academy of Sciences*, 118(10), e2015797118.
570 <https://doi.org/10.1073/pnas.2015797118>

- 571 Liang, Y., Sengupta, D., Campmier, M. J., Lunderberg, D. M., Apte, J. S., & Goldstein, A. H.
572 (2021). Wildfire smoke impacts on indoor air quality assessed using crowdsourced data
573 in California. *Proceedings of the National Academy of Sciences*, *118*(36), e2106478118.
574 <https://doi.org/10.1073/pnas.2106478118>
- 575 Liu, T., Chen, G., Chen, J., Xu, L., Li, M., Hong, Y., Chen, Y., Ji, X., Yang, C., Chen, Y.,
576 Huang, W., Huang, Q., & Wang, H. (2022). Seasonal characteristics of atmospheric
577 peroxyacetyl nitrate (PAN) in a coastal city of Southeast China: Explanatory factors and
578 photochemical effects. *Atmospheric Chemistry and Physics*, *22*(7), 4339–4353.
579 <https://doi.org/10.5194/acp-22-4339-2022>
- 580 Liu, Z., Ciais, P., Deng, Z., Lei, R., Davis, S. J., Feng, S., Zheng, B., Cui, D., Dou, X., He, P.,
581 Zhu, B., Lu, C., Ke, P., Sun, T., Yue, X., Wang, Y., Lei, Y., Zhou, H., Cai, Z., ...
582 Schellnhuber, H. J. (n.d.). *Near-real-time data captured record decline in global CO2*
583 *emissions due to COVID-19*. 45.
- 584 Liu, Z., Wang, Y., Gu, D., Zhao, C., Huey, L. G., Stickel, R., Liao, J., Shao, M., Zhu, T., Zeng,
585 L., Liu, S.-C., Chang, C.-C., Amoroso, A., & Costabile, F. (2010). Evidence of Reactive
586 Aromatics As a Major Source of Peroxy Acetyl Nitrate over China. *Environmental*
587 *Science & Technology*, *44*(18), 7017–7022. <https://doi.org/10.1021/es1007966>
- 588 Martin, R. V., Fiore, A. M., & Van Donkelaar, A. (2004). Space-based diagnosis of surface
589 ozone sensitivity to anthropogenic emissions: SURFACE OZONE SENSITIVITY TO
590 EMISSIONS. *Geophysical Research Letters*, *31*(6), n/a-n/a.
591 <https://doi.org/10.1029/2004GL019416>
- 592 Mena-Carrasco, M., Carmichael, G. R., Campbell, J. E., Zimmerman, D., Tang, Y., Adhikary,
593 B., D'allura, A., Molina, L. T., Zavala, M., Garcia, A., Flocke, F., Campos, T.,

- 594 Weinheimer, A. J., Shetter, R., Apel, E., Montzka, D. D., Knapp, D. J., & Zheng, W.
595 (2009). Assessing the regional impacts of Mexico City emissions on air quality and
596 chemistry. *Atmos. Chem. Phys.*, 13.
- 597 Miyazaki, K., Bowman, K., Sekiya, T., Eskes, H., Boersma, F., Worden, H., Livesey, N., Payne,
598 V. H., Sudo, K., Kanaya, Y., Takigawa, M., & Ogochi, K. (2020). Updated tropospheric
599 chemistry reanalysis and emission estimates, TCR-2, for 2005–2018. *Earth System
600 Science Data*, 12(3), 2223–2259. <https://doi.org/10.5194/essd-12-2223-2020>
- 601 Miyazaki, K., Bowman, K., Sekiya, T., Jiang, Z., Chen, X., Eskes, H., Ru, M., Zhang, Y., &
602 Shindell, D. (2020). Air Quality Response in China Linked to the 2019 Novel
603 Coronavirus (COVID-19) Lockdown. *Geophysical Research Letters*, 47(19).
604 <https://doi.org/10.1029/2020GL089252>
- 605 Miyazaki, K., Bowman, K., Sekiya, T., Takigawa, M., Neu, J. L., Sudo, K., Osterman, G., &
606 Eskes, H. (2021). Global tropospheric ozone responses to reduced NO_x emissions linked
607 to the COVID-19 worldwide lockdowns. *SCIENCE ADVANCES*, 15.
- 608 Miyazaki, K., Eskes, H., Sudo, K., Boersma, K. F., Bowman, K., & Kanaya, Y. (2017). Decadal
609 changes in global surface NO₂; emissions from multi-constituent satellite data
610 assimilation. *Atmospheric Chemistry and Physics*, 17(2), 807–837.
611 <https://doi.org/10.5194/acp-17-807-2017>
- 612 Nussbaumer, C. M., & Cohen, R. C. (2020). The Role of Temperature and NO_x in Ozone
613 Trends in the Los Angeles Basin. *Environmental Science & Technology*, 54(24), 15652–
614 15659. <https://doi.org/10.1021/acs.est.0c04910>
- 615 Odekanle, E. L., Fakinle, B. S., Odejobi, O. J., Akangbe, O. E., Sonibare, J. A., Akeredolu, F. A.,
616 & Oladoja, O. M. (2022). COVID-19 induced restriction in developing countries and its

- 617 impacts on pollution load: Case study of Lagos mega city. *Heliyon*, 8(8), e10402.
618 <https://doi.org/10.1016/j.heliyon.2022.e10402>
- 619 Payne, V. H., Alvarado, M. J., Cady-Pereira, K. E., Worden, J. R., Kulawik, S. S., & Fischer, E.
620 V. (2014). Satellite observations of peroxyacetyl nitrate from the Aura Tropospheric
621 Emission Spectrometer. *Atmospheric Measurement Techniques*, 7(11), 3737–3749.
622 <https://doi.org/10.5194/amt-7-3737-2014>
- 623 Payne, V. H., Fischer, E. V., Worden, J. R., Jiang, Z., Zhu, L., Kurosu, T. P., & Kulawik, S. S.
624 (2017). Spatial variability in tropospheric peroxyacetyl nitrate in the tropics from infrared
625 satellite observations in 2005 and 2006. *Atmospheric Chemistry and Physics*, 17(10),
626 6341–6351. <https://doi.org/10.5194/acp-17-6341-2017>
- 627 Payne, V. H., Kulawik, S. S., Fischer, E. V., Brewer, J. F., Huey, L. G., Miyazaki, K., Worden, J.
628 R., Bowman, K. W., Hints, E. J., Moore, F., Elkins, J. W., & Juncosa Calahorrano, J.
629 (2022). *Satellite measurements of peroxyacetyl nitrate from the Cross-Track Infrared*
630 *Sounder: Comparison with ATom aircraft measurements. Gases/Remote*
631 *Sensing/Validation and Intercomparisons.* <https://doi.org/10.5194/amt-15-3497-2022>
- 632 Penkett, S. A., & Brice, K. A. (1986). The spring maximum in photo-oxidants in the Northern
633 Hemisphere troposphere. *Nature*, 319(6055), 655–657. <https://doi.org/10.1038/319655a0>
- 634 Peralta, O., Ortíz-Alvarez, A., Torres-Jardón, R., Suárez-Lastra, M., Castro, T., & Ruíz-
635 Suárez, L. G. (2021). Ozone over Mexico City during the COVID-19 pandemic. *Science*
636 *of The Total Environment*, 761, 143183. <https://doi.org/10.1016/j.scitotenv.2020.143183>
- 637 Pollack, I. B., Ryerson, T. B., Trainer, M., Neuman, J. A., Roberts, J. M., & Parrish, D. D.
638 (2013). Trends in ozone, its precursors, and related secondary oxidation products in Los
639 Angeles, California: A synthesis of measurements from 1960 to 2010: OZONE TRENDS

- 640 IN LA FROM 1960 TO 2010. *Journal of Geophysical Research: Atmospheres*, 118(11),
641 5893–5911. <https://doi.org/10.1002/jgrd.50472>
- 642 Qiu, Y., Ma, Z., & Li, K. (2019). A modeling study of the peroxyacetyl nitrate (PAN) during a
643 wintertime haze event in Beijing, China. *Science of The Total Environment*, 650, 1944–
644 1953. <https://doi.org/10.1016/j.scitotenv.2018.09.253>
- 645 Qiu, Y., Ma, Z., Li, K., Lin, W., Tang, Y., Dong, F., & Liao, H. (2020). Markedly Enhanced
646 Levels of Peroxyacetyl Nitrate (PAN) During COVID-19 in Beijing. *Geophysical
647 Research Letters*, 47(19). <https://doi.org/10.1029/2020GL089623>
- 648 Randerson, J., van der verf, G., Gilglio, L., Collatz, G., & Kasibhatla, P. (2018). Global Fire
649 Emissions Database, Version 4, (GFEDv4), ORNL DAAC. *Oak Ridge, Tennessee, USA*.
- 650 Rappenglück, B., Melas, D., & Fabian, P. (2003). Evidence of the impact of urban plumes on
651 remote sites in the Eastern Mediterranean. *Atmospheric Environment*, 37(13), 1853–
652 1864. [https://doi.org/10.1016/S1352-2310\(03\)00065-7](https://doi.org/10.1016/S1352-2310(03)00065-7)
- 653 Roberts, J. M. (2007). PAN and Related Compounds. In R. Koppmann (Ed.), *Volatile Organic
654 Compounds in the Atmosphere* (pp. 221–268). Blackwell Publishing Ltd.
655 <https://doi.org/10.1002/9780470988657.ch6>
- 656 Saxena, P., Sonwani, S., Srivastava, A., Jain, M., Srivastava, A., Bharti, A., Rangra, D., Mongia,
657 N., Tejan, S., & Bhardwaj, S. (2021). Impact of crop residue burning in Haryana on the
658 air quality of Delhi, India. *Heliyon*, 7(5), e06973.
659 <https://doi.org/10.1016/j.heliyon.2021.e06973>
- 660 Schroeder, J. R., Cai, C., Xu, J., Ridley, D., Lu, J., Bui, N., Yan, F., & Avise, J. (2022).
661 Changing ozone sensitivity in the South Coast Air Basin during the COVID-19 period.

- 662 *Atmospheric Chemistry and Physics*, 22(19), 12985–13000. <https://doi.org/10.5194/acp->
663 22-12985-2022
- 664 Sharma, S., Zhang, M., Anshika, Gao, J., Zhang, H., & Kota, S. H. (2020). Effect of restricted
665 emissions during COVID-19 on air quality in India. *Science of The Total Environment*,
666 728, 138878. <https://doi.org/10.1016/j.scitotenv.2020.138878>
- 667 Shen, L., Jacob, D. J., Zhu, L., Zhang, Q., Zheng, B., Sulprizio, M. P., Li, K., De Smedt, I.,
668 González Abad, G., Cao, H., Fu, T., & Liao, H. (2019). The 2005–2016 Trends of
669 Formaldehyde Columns Over China Observed by Satellites: Increasing Anthropogenic
670 Emissions of Volatile Organic Compounds and Decreasing Agricultural Fire Emissions.
671 *Geophysical Research Letters*, 46(8), 4468–4475. <https://doi.org/10.1029/2019GL082172>
- 672 Shi, X., & Brasseur, G. P. (2020). The Response in Air Quality to the Reduction of Chinese
673 Economic Activities During the COVID-19 Outbreak. *Geophysical Research Letters*,
674 47(11). <https://doi.org/10.1029/2020GL088070>
- 675 Shogrin, M. J. (2023). *CrIS PANs megacity dataset for São Paulo and Lagos* [..Csv]. Dryad.
676 <https://doi.org/10.5061/dryad.wpzgmsbtk>
- 677 Shogrin, M. J., Payne, V. H., Kulawik, S. S., Miyazaki, K., & Fischer, E. V. (2023).
678 Measurement report: Spatiotemporal variability of peroxy acyl nitrates (PANs) over
679 Mexico City from TES and CrIS satellite measurements. *Atmospheric Chemistry and*
680 *Physics*, 23(4), 2667–2682. <https://doi.org/10.5194/acp-23-2667-2023>
- 681 Sicard, P., De Marco, A., Agathokleous, E., Feng, Z., Xu, X., Paoletti, E., Rodriguez, J. J. D., &
682 Calatayud, V. (2020). Amplified ozone pollution in cities during the COVID-19
683 lockdown. *Science of The Total Environment*, 735, 139542.
684 <https://doi.org/10.1016/j.scitotenv.2020.139542>

- 685 Sillman, S., & West, J. J. (2009). Reactive nitrogen in Mexico City and its relation to ozone-
686 precursor sensitivity: Results from photochemical models. *Atmos. Chem. Phys.*, 13.
- 687 Singh, H. B., & Hanst, P. L. (1981). Peroxyacetyl nitrate (PAN) in the unpolluted atmosphere:
688 An important reservoir for nitrogen oxides. *Geophysical Research Letters*, 8(8), 941–944.
689 <https://doi.org/10.1029/GL008i008p00941>
- 690 Singh, H. B., Salas, L. J., & Viezee, W. (1986). Global distribution of peroxyacetyl nitrate.
691 *Nature*, 321(6070), 588–591. <https://doi.org/10.1038/321588a0>
- 692 Souri, A. H., Johnson, M. S., Wolfe, G. M., Crawford, J. H., Fried, A., Wisthaler, A., Brune, W.
693 H., Blake, D. R., Weinheimer, A. J., Verhoelst, T., Compernelle, S., Pinardi, G.,
694 Vigouroux, C., Langerock, B., Choi, S., Lamsal, L., Zhu, L., Sun, S., Cohen, R. C., ...
695 Chance, K. (2023). Characterization of errors in satellite-based HCHO/NO₂
696 tropospheric column ratios with respect to chemistry, column-to-PBL translation, spatial
697 representation, and retrieval uncertainties. *Atmospheric Chemistry and Physics*, 23(3),
698 1963–1986. <https://doi.org/10.5194/acp-23-1963-2023>
- 699 Souri, A. H., Nowlan, C. R., Wolfe, G. M., Lamsal, L. N., Chan Miller, C. E., Abad, G. G., Janz,
700 S. J., Fried, A., Blake, D. R., Weinheimer, A. J., Diskin, G. S., Liu, X., & Chance, K.
701 (2020). Revisiting the effectiveness of HCHO/NO₂ ratios for inferring ozone sensitivity
702 to its precursors using high resolution airborne remote sensing observations in a high
703 ozone episode during the KORUS-AQ campaign. *Atmospheric Environment*, 224,
704 117341. <https://doi.org/10.1016/j.atmosenv.2020.117341>
- 705 Stavrakou, T., Müller, J.-F., Bauwens, M., Doumbia, T., Elguindi, N., Darras, S., Granier, C.,
706 Smedt, I. D., Lerot, C., Van Roozendaal, M., Franco, B., Clarisse, L., Clerbaux, C.,
707 Coheur, P.-F., Liu, Y., Wang, T., Shi, X., Gaubert, B., Tilmes, S., & Brasseur, G. (2021).

- 708 Atmospheric Impacts of COVID-19 on NO_x and VOC Levels over China Based on
709 TROPOMI and IASI Satellite Data and Modeling. *Atmosphere*, 12(8), 946.
710 <https://doi.org/10.3390/atmos12080946>
- 711 Steiner, A. L., Davis, A. J., Sillman, S., Owen, R. C., Michalak, A. M., & Fiore, A. M. (2010).
712 Observed suppression of ozone formation at extremely high temperatures due to chemical
713 and biophysical feedbacks. *Proceedings of the National Academy of Sciences*, 107(46),
714 19685–19690. <https://doi.org/10.1073/pnas.1008336107>
- 715 Venter, Z. S., Aunan, K., Chowdhury, S., & Lelieveld, J. (2020). COVID-19 lockdowns cause
716 global air pollution declines. *Proceedings of the National Academy of Sciences*, 117(32),
717 18984–18990. <https://doi.org/10.1073/pnas.2006853117>
- 718 Wang, L., Jin, X., Wang, Q., Mao, H., Liu, Q., Weng, G., & Wang, Y. (2020). Spatial and
719 temporal variability of open biomass burning in Northeast China from 2003 to 2017.
720 *Atmospheric and Oceanic Science Letters*, 13(3), 240–247.
721 <https://doi.org/10.1080/16742834.2020.1742574>
- 722 Wang, Q., & Li, S. (2021). Nonlinear impact of COVID-19 on pollutions – Evidence from
723 Wuhan, New York, Milan, Madrid, Bandra, London, Tokyo and Mexico City.
724 *Sustainable Cities and Society*, 65, 102629. <https://doi.org/10.1016/j.scs.2020.102629>
- 725 Warneke, C., de Gouw, J. A., Edwards, P. M., Holloway, J. S., Gilman, J. B., Kuster, W. C.,
726 Graus, M., Atlas, E., Blake, D., Gentner, D. R., Goldstein, A. H., Harley, R. A., Alvarez,
727 S., Rappenglueck, B., Trainer, M., & Parrish, D. D. (2013). Photochemical aging of
728 volatile organic compounds in the Los Angeles basin: Weekday-weekend effect: VOC
729 WEEKDAY-WEEKEND EFFECT. *Journal of Geophysical Research: Atmospheres*,
730 118(10), 5018–5028. <https://doi.org/10.1002/jgrd.50423>

- 731 WHO. (2020). *Coronavirus disease 2019 (COVID-19): Situation Report – 43*.
732 [www.who.int/docs/default-source/coronaviruse/situation-reports/20200303-sitrep-43-](http://www.who.int/docs/default-source/coronaviruse/situation-reports/20200303-sitrep-43-covid-19.pdf?sfvrsn=2c21c09c_2)
733 [covid-19.pdf?sfvrsn=2c21c09c_2](http://www.who.int/docs/default-source/coronaviruse/situation-reports/20200303-sitrep-43-covid-19.pdf?sfvrsn=2c21c09c_2).
- 734 Worden, H. M., Francis, G. L., Kulawik, S. S., Bowman, K. W., Cady-Pereira, K., Fu, D.,
735 Hegarty, J. D., Kantchev, V., Luo, M., Payne, V. H., Worden, J. R., Commane, R., &
736 McKain, K. (2022). *TROPES/CrIS carbon monoxide profile validation with NOAA*
737 *GML and ATom in situ aircraft observations* [Preprint]. Gases/Remote
738 Sensing/Validation and Intercomparisons. <https://doi.org/10.5194/amt-2022-128>
- 739 Yin, L., Du, P., Zhang, M., Liu, M., Xu, T., & Song, Y. (2019). Estimation of emissions from
740 biomass burning in China (2003–2017) based on MODIS fire radiative energy data.
741 *Biogeosciences*, *16*(7), 1629–1640. <https://doi.org/10.5194/bg-16-1629-2019>
- 742 Yoshitomi, M., Wild, O., & Akimoto, H. (2011). *Contributions of regional and intercontinental*
743 *transport to surface ozone in Tokyo* [Preprint]. Gases/Atmospheric
744 Modelling/Troposphere/Chemistry (chemical composition and reactions).
745 <https://doi.org/10.5194/acpd-11-10403-2011>
- 746 Zhang, B., Zhao, B., Zuo, P., Huang, Z., & Zhang, J. (2017). Ambient peroxyacyl nitrate
747 concentration and regional transportation in Beijing. *Atmospheric Environment*, *166*,
748 543–550. <https://doi.org/10.1016/j.atmosenv.2017.07.053>
- 749 Zhang, B., Zhao, X., & Zhang, J. (2019). Characteristics of peroxyacetyl nitrate pollution during
750 a 2015 winter haze episode in Beijing. *Environmental Pollution*, *244*, 379–387.
751 <https://doi.org/10.1016/j.envpol.2018.10.078>
- 752 Zhang, G., Mu, Y., Zhou, L., Zhang, C., Zhang, Y., Liu, J., Fang, S., & Yao, B. (2015a).
753 Summertime distributions of peroxyacetyl nitrate (PAN) and peroxypropionyl nitrate

- 754 (PPN) in Beijing: Understanding the sources and major sink of PAN. *Atmospheric*
755 *Environment*, 103, 289–296. <https://doi.org/10.1016/j.atmosenv.2014.12.035>
- 756 Zhang, G., Mu, Y., Zhou, L., Zhang, C., Zhang, Y., Liu, J., Fang, S., & Yao, B. (2015b).
757 Summertime distributions of peroxyacetyl nitrate (PAN) and peroxypropionyl nitrate
758 (PPN) in Beijing: Understanding the sources and major sink of PAN. *Atmospheric*
759 *Environment*, 103, 289–296. <https://doi.org/10.1016/j.atmosenv.2014.12.035>
- 760 Zhang, G., Xia, L., Zang, K., Xu, W., Zhang, F., Liang, L., Yao, B., Lin, W., & Mu, Y. (2020).
761 The abundance and inter-relationship of atmospheric peroxyacetyl nitrate (PAN),
762 peroxypropionyl nitrate (PPN), O₃, and NO_y during the wintertime in Beijing, China.
763 *Science of The Total Environment*, 718, 137388.
764 <https://doi.org/10.1016/j.scitotenv.2020.137388>
- 765 Zhang, J., Lim, Y.-H., Andersen, Z. J., Napolitano, G., Taghavi Shahri, S. M., So, R., Plucker,
766 M., Danesh-Yazdi, M., Cole-Hunter, T., Therning Jørgensen, J., Liu, S., Bergmann, M.,
767 Jayant Mehta, A., H. Mortensen, L., Requia, W., Lange, T., Loft, S., Kuenzli, N.,
768 Schwartz, J., & Amini, H. (2022). Stringency of COVID-19 Containment Response
769 Policies and Air Quality Changes: A Global Analysis across 1851 Cities. *Environmental*
770 *Science & Technology*, 56(17), 12086–12096. <https://doi.org/10.1021/acs.est.2c04303>
- 771 Zhao, Y., Xu, R., Xu, Z., Wang, L., & Wang, P. (2022). Temporal and Spatial Patterns of
772 Biomass Burning Fire Counts and Carbon Emissions in the Beijing–Tianjin–Hebei
773 (BTH) Region during 2003–2020 Based on GFED4. *Atmosphere*, 13(3), 459.
774 <https://doi.org/10.3390/atmos13030459>
- 775 Zhu, L., Fischer, E. V., Payne, V. H., Worden, J. R., & Jiang, Z. (2015). TES observations of the
776 interannual variability of PAN over Northern Eurasia and the relationship to springtime

777 fires. *Geophysical Research Letters*, 42(17), 7230–7237.

778 <https://doi.org/10.1002/2015GL065328>

779 Zhu, L., Payne, V. H., Walker, T. W., Worden, J. R., Jiang, Z., Kulawik, S. S., & Fischer, E. V.

780 (2017). PAN in the eastern Pacific free troposphere: A satellite view of the sources,

781 seasonality, interannual variability, and timeline for trend detection. *Journal of*

782 *Geophysical Research: Atmospheres*, 122(6), 3614–3629.

783 <https://doi.org/10.1002/2016JD025868>

784

1 **Changes to Peroxyacyl Nitrates (PANs) over Megacities in Response to COVID-19**
2 **Tropospheric NO₂ Reductions Observed by the Cross-track Infrared Sounder (CrIS)**
3 **Madison J. Shogrin¹, Vivienne H. Payne², Susan S. Kulawik³, Kazuyuki Miyazaki², and**
4 **Emily V. Fischer¹**

5 ¹Colorado State University, Department of Atmospheric Science, Fort Collins, CO, USA.

6 ²Jet Propulsion Laboratory, California Institute of Technology, Pasadena CA, USA.

7 ³Bay Area Environmental Research Institute, Petaluma, CA, USA.

8 Corresponding author: Madison J. Shogrin (madison.shogrin@colostate.edu)

9 **Key Points:**

- 10 • There are pronounced seasonal cycles of PANs over each megacity that align with
11 seasonal maximums in photochemistry.
- 12 • Observed free tropospheric mixing ratios of PANs during COVID-19 were significantly
13 different over two out of eight surveyed megacities.
- 14 • Sensitivity of free tropospheric PANs to the abundance of precursors is seasonally
15 dependent in some locations.

16 Abstract

17 The COVID-19 pandemic perturbed air pollutant emissions as cities shutdown worldwide. Peroxyacyl
18 nitrates (PANs) are important tracers of photochemistry that are formed through the oxidation of non-
19 methane volatile organic compounds (NMVOCs) in the presence of nitrogen oxide radicals ($\text{NO}_x = \text{NO} +$
20 NO_2). We use satellite measurements of free tropospheric PANs from the S-NPP Cross-Track Infrared
21 Sounder (CrIS) over eight of the world's megacities: Mexico City, Beijing, Los Angeles, Tokyo, São
22 Paulo, Delhi, Lagos, and Karachi. We quantify the seasonal cycle of PANs over these megacities and find
23 seasonal maxima in PANs correspond to seasonal peaks in local photochemistry. CrIS is used to explore
24 changes in PANs in response to the COVID-19 lockdowns. Statistically significant changes to PANs
25 occurred over two megacities: Los Angeles (PAN decreased) and Beijing (PAN increased). Our analysis
26 suggests that large perturbations in NO_x may not result in significant declines in NO_x export potential of
27 megacities.

28 Plain Language Summary

29 The COVID-19 pandemic led to the lockdown of urban centers worldwide, drastically perturbing the
30 concentrations of global air pollutants. Peroxyacyl nitrates (PANs) are important photochemical
31 pollutants formed from reactions between NO_x and volatile organic compounds (VOCs), which were
32 substantially reduced during the pandemic. We use satellite measurements of PANs from the Suomi-
33 National Polar-orbiting Partnership (S-NPP) Cross-Track Infrared Sounder (CrIS) in the free troposphere
34 over and surrounding eight of the world's megacities: Mexico City, Beijing, Los Angeles, Tokyo, São
35 Paulo, Delhi, Lagos, and Karachi. Seasonal cycles of PANs are pronounced and the seasonal maxima
36 correspond to seasonal peaks in local photochemistry. Significant changes to PANs in response to
37 COVID-19 occurred over two out of the eight cities: Los Angeles (PANs decreased) and Beijing (PANs
38 increased). Our results indicate that large changes in NO_x may not result in equally significant changes to
39 PANs and the NO_x export potential of megacities.

40 1 Introduction

41 To slow the spread of the 2019 novel coronavirus (COVID-19), urban centers across the globe
42 partially shut down for various amounts of time (Chinazzi et al., 2020; WHO, 2020). While the timing
43 differed for each urban region, a consequence of these bursts of reduced economic activity was a radical
44 decrease in the emissions of many primary air pollutants. Reductions in global and regional particulate
45 matter, nitrogen oxides ($\text{NO}_x = \text{NO} + \text{NO}_2$), carbon dioxide (CO_2), and other trace gasses associated with
46 the COVID-19 pandemic have been documented (Bauwens et al., 2020; Z. Liu et al., n.d.; Miyazaki,
47 Bowman, Sekiya, Jiang, et al., 2020; Miyazaki et al., 2021; Odekanle et al., 2022; Sharma et al., 2020;
48 Shi & Brasseur, 2020; Venter et al., 2020; J. Zhang et al., 2022) Less is understood about changes to
49 secondary pollutants as they respond non-linearly to changes in precursor emissions, and their production
50 and lifetime also depend on environmental conditions (e.g., Stavrou et al., 2021). For example, both
51 increases and decreases in surface ozone (O_3) have been documented in urban areas during the COVID-
52 19 pandemic despite decreases in precursor emissions (e.g., Le et al., 2020; Miyazaki et al., 2021; Qiu et
53 al., 2020; Shi & Brasseur, 2020; Sicard et al., 2020).

54 Peroxyacyl nitrates (PANs) are important photochemically-produced species that are formed
55 alongside O_3 in polluted environments by the oxidation of non-methane volatile organic compounds
56 (NMVOCs) in the presence of NO_x (Fischer et al., 2014; Gaffney et al., 1989; Roberts, 2007; Singh et al.,
57 1986; Singh & Hanst, 1981). PANs are considered to be a sensitive tracer of photochemistry (e.g.,
58 Coggon et al., 2021; Rappenglück et al., 2003). Formation and decomposition of PANs can impact the
59 production of O_3 (e.g. Steiner et al., 2010), the production of PANs acts as an indicator of regional
60 photochemistry (Sillman & West, 2009), and the concentration of PANs can be used to gauge
61 effectiveness of O_3 -control strategies (Gaffney et al., 1989). PANs respond to precursor emissions non-
62 linearly and have been shown to be more sensitive to changes in NMVOCs versus changes in NO_x for

63 many regions of the global atmosphere (Fischer et al., 2014) and in some urban regions (T. Liu et al.,
64 2022).

65 The lifetime of PANs against thermal decomposition is strongly dependent on temperature, where
66 PANs are thermally unstable in the lower troposphere (lifetime on the order of hours at 20°C), but have a
67 lifetime >1 month at temperatures characteristic of the mid-troposphere (Honrath et al., 1996). When
68 transported from polluted continental regions to the remote troposphere, PANs serve as the principal
69 reservoir species for NO_x and can contribute to efficient production of downwind O₃ in NO_x limited
70 conditions (Fischer et al., 2014; Mena-Carrasco et al., 2009). The distribution of O₃ in the remote
71 atmosphere would be substantially different without PAN chemistry (e.g., Jiang et al., 2016). There have
72 been major changes in NO_x and VOC emissions in urban areas in recent decades, elevating the need for
73 continued and extended observations of photochemically-relevant species in urban regions. In situ
74 measurements of PANs have been collected for select urban areas for select seasons (Gaffney et al., 1989;
75 Qiu et al., 2019; G. Zhang et al., 2015a), though observations are generally sparse.

76 Here we present new satellite observations of PANs over eight megacities. We utilize
77 measurements from the Suomi-National Polar-orbiting Partnership (S-NPP) Cross-Track Infrared
78 Sounder (CrIS) and other complimentary satellite and reanalysis datasets to document the seasonal cycles
79 of PANs over select megacities and the response of PANs to COVID-19 induced reductions of precursor
80 concentrations in these locations.

81

82 **2 Materials and Methods**

83 **2.1 CrIS Observations**

84 We use observations of free tropospheric PANs and CO from the CrIS instrument, a nadir
85 viewing Fourier transform spectroradiometer currently flying on the S-NPP satellite. The datasets used
86 here were produced under the NASA Tropospheric Ozone and Precursors from Earth System Sounding
87 (TROPESS) project (Bowman, 2021c, 2021k, 2021o, 2021a, 2021e, 2021i, 2021l, 2021p, 2021d, 2021j,
88 2021b, 2021f, 2021c; Shogrin, 2023). Information on the CrIS PANs retrieval algorithm and validation
89 against aircraft observations can be found in Payne et al. (2022). The validation efforts for the CrIS PANs
90 product suggest a single sounding uncertainty of around 0.08 ppbv that reduces with averaging to an
91 approximate floor of 0.05 ppbv and demonstrates the ability of CrIS to capture variation in the
92 “background” PANs over remote regions (Payne et al., 2022). The CrIS CO algorithm is described in Fu
93 et al. (2016) and validation is presented in Worden et al. (2022). A single sounding uncertainty for CrIS
94 CO retrievals is on the order of 6-10% (Worden et al., 2022) and this is expected to reduce with
95 averaging. Our analysis uses the column average PANs volume mixing ratio (VMR) between 825 and
96 215 hPa. CrIS PANs retrievals have peak sensitivity in the free troposphere (~680 hPa) and the sensitivity
97 decreases rapidly near the surface. At most, CrIS PANs retrievals have 1 degree of freedom for signal
98 (DOF), meaning this product does not include information about the vertical distribution of PANs in the
99 atmosphere. The spectral feature utilized by CrIS for retrieval of PANs is centered at 790 cm⁻¹. This
100 infrared spectral feature appears in the spectra of all PANs at essentially the same frequency, so CrIS
101 measurements include all PAN species (i.e., they include propionyl peroxy nitrate (PPN;
102 CH₃CH₂C(O)OONO₂), methacryloyl peroxy nitrate (MPAN; CH₂C(CH₃)C(O)OONO₂), etc.) in addition
103 to peroxyacetyl nitrate (PAN; CH₃C(O)O₂NO₂). We also use a tropospheric average of CrIS CO between
104 825 hPa and 215 hPa. Our analysis focuses on CrIS PANs over and around 9 megacities utilizing CrIS
105 CO to contextualize seasonal enhancements in PANs.

106

107 PAN observations from nadir-viewing satellites include those from the Tropospheric Emission
108 Spectrometer (TES) (Payne et al., 2014) as well as meteorological sounders namely the Infrared
109 Atmospheric Sounding Interferometer (IASI) (Franco et al., 2018) and CrIS (Payne et al., 2022). Studies
110 observing PAN from space thus far have focused on PAN enhancements associated with fires (Alvarado

111 et al., 2011; Clarisse et al., 2011; Juncosa Calahorrano et al., 2021) and the global distribution of PAN
112 and its role in the long range transport of O₃ (Fischer et al., 2018; Jiang et al., 2016; Payne et al., 2017;
113 Zhu et al., 2015; 2017). Although TES had provided a set of special observations over select megacities
114 (Cady-Pereira et al., 2017; Shogrin et al., 2023), the spatial and temporal coverage of this dataset is
115 somewhat limited. Here, we utilize the more comprehensive spatial and temporal coverage of CrIS to
116 explore the spatiotemporal distribution of PANs over and around megacities.

117 118 **2.2 Ozone Monitoring Instrument (OMI) Observations**

119
120 We use Level 3 NO₂ tropospheric column measurements from NASA Aura-OMI to identify
121 months with anomalously low NO₂ columns associated with COVID in 2020. We use the Quality
122 Assurance for Essential Climate Variables (QA4ECV) NO₂ Level 3 product described in Boersma et al.
123 (2018) as this is the most recently updated data product. OMI NO₂ L3 monthly mean data used in this
124 study is provided on a global 0.125° x 0.125° grid and can be found on the TEMIS database (Boersma et
125 al., 2017b).

126
127 We use Level 3 (L3) HCHO tropospheric column measurements, also from OMI, to contextualize
128 changes in monthly VOC concentrations in megacities during the period of anomalously low tropospheric
129 NO₂. Space-based observations of HCHO are used as an indicator of VOC emissions (De Smedt et al.,
130 2008; Shen et al., 2019). HCHO is also processed using the QA4ECV algorithm consistently with the NO₂
131 data used in this study. HCHO L3 monthly mean data is also provided on a global 0.125° x 0.125° grid
132 and can also be found on the TEMIS database (De Smedt et al., 2017).

133 134 **2.3 Chemical Reanalysis Product**

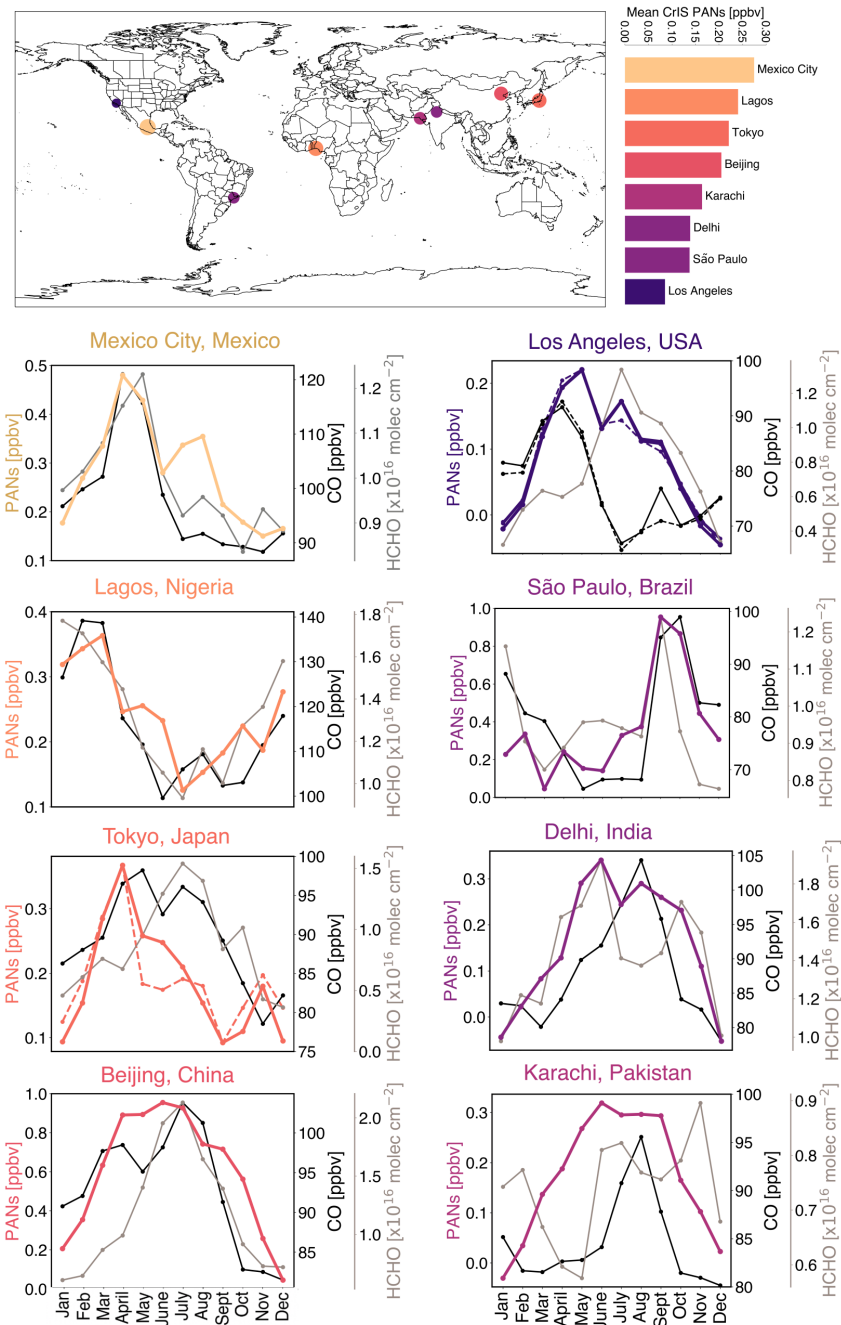
135
136 We use NO_x emission reanalysis data to also place changes to PANs in the context of NO_x emission flux
137 reductions in megacities associated with COVID-19. NO_x emissions are from an assimilation of multi-
138 species satellite observations (O₃, CO, NO₂, HNO₃, and SO₂) in the Tropospheric Chemistry Reanalysis
139 version 2 (TCR-2) framework (Miyazaki et al., 2020; <https://doi.org/10.25966/9qgv-fe81>). NO_x
140 emissions are constrained by tropospheric column NO₂ retrievals from the QA4ECV version 1.1 Level 2
141 products from OMI and Global Ozone Monitoring Experiment 2 (GOME-2) (Boersma et al., 2017a,
142 2017b). A priori emissions are from HTAP version 2 for 2010 (Janssens-Maenhout et al., 2015), Global
143 Fire Emissions Database (GFED) version 4 (Randerson et al., 2018), and the Global Emissions Inventory
144 Activity (GEIA) (Graedel et al., 1993). The reanalysis fields have been evaluated against independent
145 observations on regional and global scales (Miyazaki et al., 2020). NO_x emissions for 2020 used in our
146 analysis are estimated using business as usual (BAU) emissions added to the estimated COVID-19
147 emissions anomaly described in Miyazaki et al. (2021). While the observed NO₂ concentrations are
148 affected by meteorological concentrations, their effect is already taken into account when estimating the
149 NO_x emissions (Miyazaki et al., 2017; 2020)

150
151
152

153

154 **3 Results and discussion**

155 **3.1 Seasonal Cycles of PANs, CO, and HCHO in megacities**



156

157

158 **Figure 1.** Top: Map shows mean detected CrIS PANs for the entire study period. The scale to the right of
 159 the map ranks the cities using the mean PANs. Dot sizing is indicative of abundance of mean PANs.

160 Seasonal cycles of CrIS PANs [ppbv] (color denoted in color bar, dashed denotes median values), CrIS
 161 tropospheric CO [ppbv] (dark grey), and OMI HCHO tropospheric column average [$\times 10^{16}$ molecules cm^{-2}]

162 (lighter grey) for eight megacities. Note: scales vary for each plot. Monthly means include data from
163 January 2016 to May 2021.

164
165 Figure 1 displays the mean seasonal cycles for CrIS PANs, CrIS CO, and OMI HCHO for eight
166 different global megacities from 2016-2021. Figure 1 helps identify periods in the annual cycle with
167 production of PANs and values of PANs above a threshold where CrIS is able to provide quantitative
168 information. For most cities, NO₂ changes from COVID-19 coincide with periods where PANs are above
169 the CrIS detection limit (Section 2.1) and conditions support photochemical production.

170 All but two selected megacities experience a springtime maxima in PANs. The seasonal
171 springtime maximum in PANs is attributed to an increase in photochemical activity at a time when PANs
172 have a relatively long lifetime against thermal decomposition (Brice et al., 1988; Fischer et al., 2014;
173 Penkett & Brice, 1986). Seasonal maxima occur in March, April, and/or May for northern hemisphere
174 megacities (Mexico City, Los Angeles (LA), Tokyo, Delhi, and Lagos), and in September for São Paulo
175 (23.56°S), the beginning of austral spring. Over Lagos (6.52°N) PANs begin increasing towards the end
176 of the calendar year and maximize in March or April. In addition to a springtime maxima, PANs over
177 Beijing (39.92°N) and Karachi (24.86°N) remain elevated through the summer (April-September).
178 Though it has a springtime maxima, Delhi (28.71°N) has a comparably wide seasonal cycle in PANs.
179 Mexico City, LA, and Tokyo also show an additional period of elevated PANs later in the year.

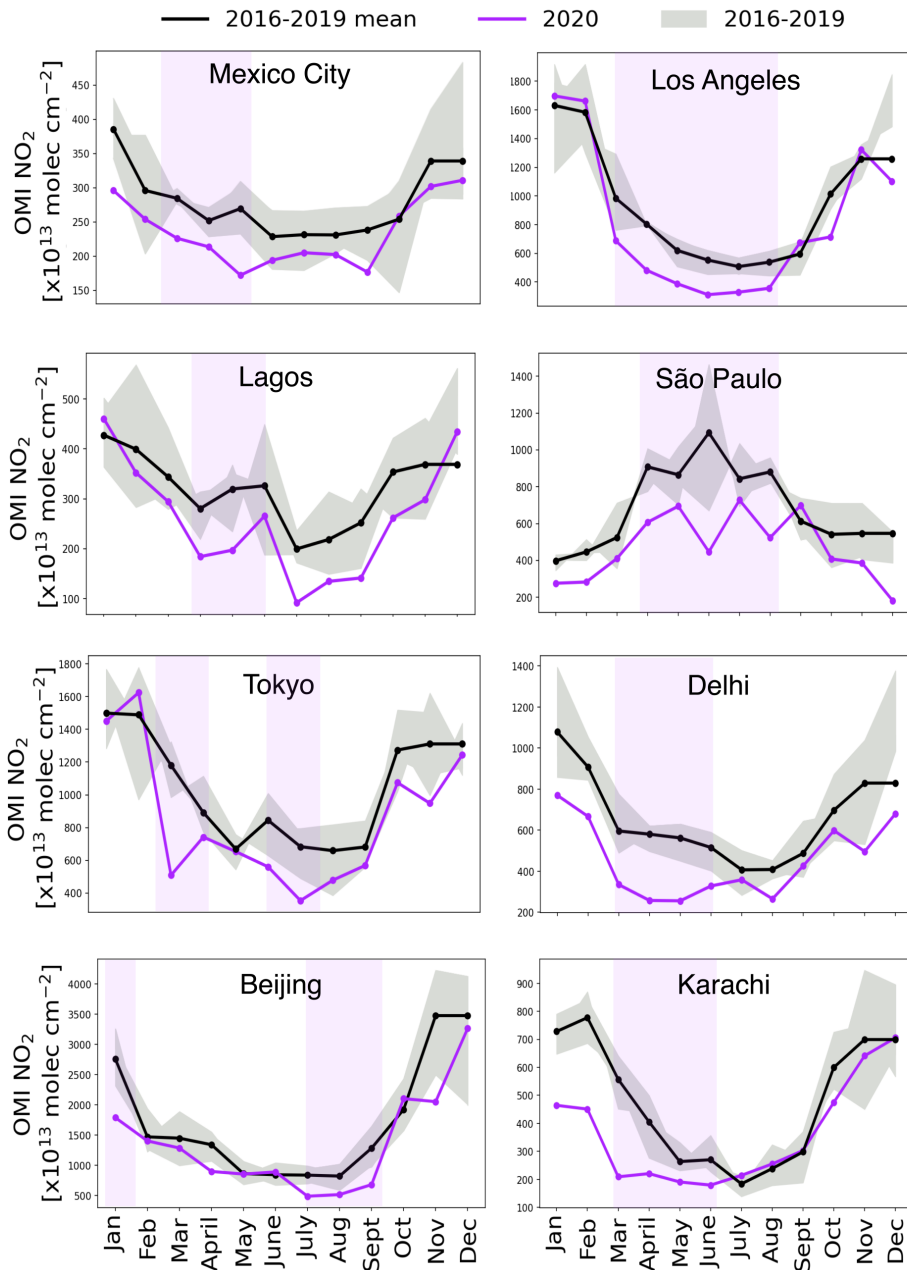
180 PANs over each megacity reflect a combination of sources and meteorological conditions, but the
181 extent of the published literature on air pollutants in each megacity differs widely. Here we focus our
182 discussion on LA, Beijing, and to a more limited extent, Tokyo, Delhi, and Lagos.

183 There is a longstanding effort to attribute and control O₃ and other photochemical pollutants in
184 LA (Langford et al., 2010; Nussbaumer & Cohen, 2020; Pollack et al., 2013; Warneke et al., 2013). CrIS
185 data indicate that the seasonal cycle in PANs over LA is distinct from both HCHO and surface O₃ (not
186 shown); tropospheric column HCHO and surface O₃ have broad maxima extending from April through
187 October and June through October, respectively. Increasing temperatures during the summer decrease the
188 lifetime of PANs due to thermal decomposition and decrease the ratio of free tropospheric PANs to
189 surface O₃. The secondary and tertiary peaks in monthly mean PANs over LA in July and September are
190 driven by wildfire smoke transported into the LA Basin in 2018 and 2020, respectively (Liang et al.,
191 2021). Wildfire impacts in September 2020 also drive the peak in September CO; note the difference
192 between the mean and median as these peaks are not evident in the median (dashed) CO and PANs for
193 these months.

194 Information on PANs within and around Beijing is growing rapidly (e.g., Z. Liu et al., 2010; B.
195 Zhang et al., 2017, 2019). In Beijing, surface O₃ and tropospheric column HCHO have seasonal maxima
196 in summer months (JJA), corresponding to the seasonal maximum in CrIS PANs (Figure 1) and recorded
197 surface observations of PAN and PPN (B. Zhang et al., 2017; G. Zhang et al., 2015b). Ground-level PAN
198 is also elevated during winter haze events in Beijing (Li et al., 2021; Qiu et al., 2019; B. Zhang et al.,
199 2019; G. Zhang et al., 2020). CrIS observes elevated CO over Beijing in March and April, consistent with
200 a seasonal peak in local fire activity in northeast China (Feng et al., 2015; L. Wang et al., 2020; Yin et al.,
201 2019; Zhao et al., 2022).

202 Tokyo has a seasonal spring maximum in photochemical species from both local and distant (*i.e.*,
203 China and Korea) sources of precursors (Lee et al., 2021; Yoshitomi et al., 2011). Delhi has a humid
204 subtropical/semi-arid climate and air pollution is strongly influenced by the Indian monsoon (Gurjar et al.,
205 2016). The monsoon season lasts from July-September and the dry season is considered to be September-
206 June. CrIS observes elevated PANs over Delhi from April to October; on average PANs remain elevated
207 through the monsoon season. Crop residue burning in April-May and October-November can deteriorate
208 air quality in the Delhi metropolitan area (Saxena et al., 2021). These periods correspond with periods of
209 elevated PANs and tropospheric column HCHO. Lagos surface O₃ increases seasonally during the dry
210 season (Abdul Raheem et al., 2009). This is consistent with CrIS observations of PANs and CO, which
211 increase and decrease with the respective dry and wet seasons.

212

213
2143.2 2020 NO₂ Anomalies

215
216 **Figure 2.** OMI NO₂ tropospheric column monthly means for 9 megacities. The area used for each city is
217 the same area around the urban area of each city used for CrIS selection and this information is provided
218 in Table 1. 2020 is shown in purple. The mean of 2016-2019 is shown in bold black. Months with
219 substantial NO₂ declines in 2020 have been highlighted in purple shading and these time frames are used
220 in the subsequent analysis presented in Figure 3.

221
222 Major changes in NO_x emissions and tropospheric NO₂ column abundances have been documented
223 worldwide for different periods of the COVID-19 pandemic (Bauwens et al., 2020; Berman & Ebisu,

224 2020; J. Zhang et al., 2022). For the analysis presented here, we identify periods where 1) the monthly
 225 mean NO₂ column during 2020 was at least 15% below the corresponding monthly mean for 2016-2019
 226 (black line in Figure 2), and 2) the monthly mean PANs mixing ratio are at least 0.05 ppbv (Figure 1). We
 227 only consider times in the seasonal cycle where mixing ratios of PANs are at least 0.05 ppbv because this
 228 corresponds with the uncertainty discussed in Section 2.1 and Payne et al. (2022). The months that meet
 229 these criteria are highlighted by the light purple shading in Figure 2. The 2020 monthly mean NO₂
 230 column density associated with these shaded periods is at least 15% less than the mean of the
 231 corresponding months for the period 2016-2019. Periods of lower observed NO₂ often do not exactly
 232 coincide with the COVID-19 government-enforced lockdowns, as reduced traffic was often observed
 233 prior to government-imposed stay-at-home orders.

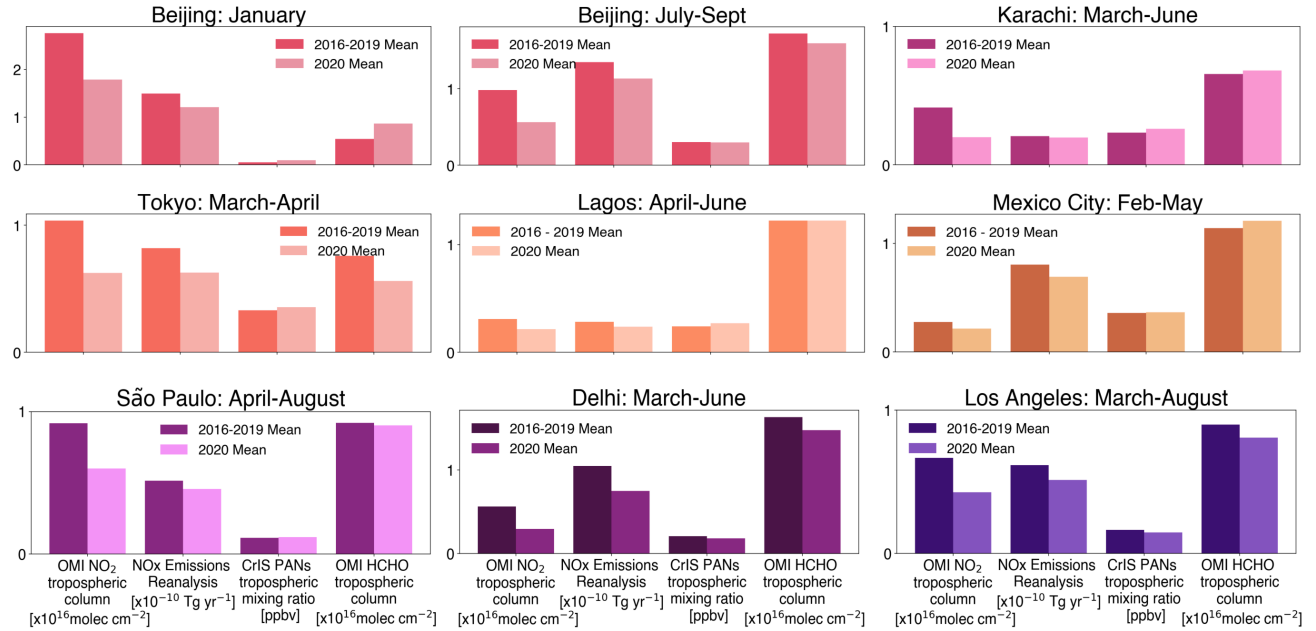
234
 235 **Table 1.** Changes to Chemical Species during Respective Time Periods.
 236

City	Monthly mean time period	NO ₂ change (%)	NO _x change (%)	HCHO change (%)	PANs change (%)	P-value
Mexico City	February-May	-22%	-14%	5.6%	1.8%	0.45
Beijing	January	-35%	-19%	59%	80%	0.03
Beijing	July-September	-40%	-16%	-7.6%	-1.9%	0.31
Tokyo	March-April	-40%	-23%	-26%	6.9%	0.11
Tokyo	June-July	-40%	-15%	-43%	-0.9%	0.44
Los Angeles	March-August	-36%	-17%	-10%	-11%	0.06
São Paulo	April-August	-35%	-11%	-1.7%	3.7%	0.33
Delhi	March-June	-48%	-28%	-9.6%	-20%	0.33
Lagos	April-June	-35%	-16%	-0.08%	11%	0.33
Karachi	March-June	-52%	-5%	3.6%	12%	0.14

237
 238 **Table 1.** Periods of significant NO₂ decline based on tropospheric column OMI NO₂ monthly means
 239 shown in Figure 2. Percent change represents the change in 2020 values relative to the mean of 2016-
 240 2019 for the respective time periods. Percent change in PANs were calculated using daily means during
 241 the months of NO₂ anomaly. P-values are from Mann-Whitney u test. A negative percent change signifies
 242 a decline in 2020 relative to the same months in prior years; likewise, positive percent changes signify an
 243 increase.
 244
 245
 246
 247
 248
 249
 250
 251
 252
 253
 254

255

3.3 Impacts of COVID-19 NO_x reductions on PANs over megacities

256
257

258 **Figure 3.** Bar charts comparing monthly means for specified months of OMI NO₂ tropospheric columns
 259 [$\times 10^{16}$ molecules cm^{-2}], NO_x emissions from the Tropospheric Chemical Reanalysis [$\times 10^{-10}$ Tg yr^{-1}], CrIS
 260 free troposphere PANs [ppbv], and OMI HCHO tropospheric columns [$\times 10^{16}$ molecules cm^{-2}] for each
 261 megacity. Means of monthly means for specified periods in 2020 (shown in Figure 2 and listed in Table
 262 1) are plotted in the lighter colors and means of 2016-2019 are plotted in the darker colors. We performed
 263 a Mann-Whitney u-test to test the significance of changes to PANs during the respective time periods of
 264 COVID-19 NO₂ perturbations listed in Table 1; 2020 was compared to the same time period from 2016-
 265 2019. We set our alpha at 0.1, so p values < 0.1 are considered significant and receive more discussion.
 266

267
268

269 Figure 3 shows that while there were large decreases in NO₂ declines at some point in 2020, this
 270 did not yield a similarly large change in free tropospheric PANs for each region. Most megacities
 271 surveyed did not experience significant change in PANs at the 90% confidence level, except for LA,
 272 which experienced a significant decline, and Beijing in winter, which experienced a significant increase.
 273 We expect that PANs (and the sensitivity of CrIS) would also respond to other environmental factors
 274 including temperature; we analyze two possible environmental indicators: 2 meter air temperature and
 275 500 hPa air temperature changes between the two respective periods over each of the megacities using
 276 MERRA-2 Reanalysis monthly mean product (Global Modeling and Assimilation Office (GMAO), 2015;
 277 DOI:10.5067/AP1B0BA5PD2K). We find no significant change in mean temperature at either pressure
 278 level between 2020 and corresponding months during the prior 4 years. Thus temperature was likely not a
 279 significant factor driving anomalies in PANs during the extended periods of NO_x perturbations
 280 highlighted in Figure 2. PANs have been used to gauge effectiveness of O₃-control strategies (*e.g.*,
 281 Gaffney et al., 1989). The tropospheric column ratios of HCHO to NO₂ have been used as a qualitative
 282 indicator of NO_x sensitive versus NO_x saturated (VOC-limited) regimes (*e.g.*, Jin et al., 2017; Martin et
 283 al., 2004; Sourì et al., 2023). Threshold values vary by location (Sourì et al., 2020), but higher (lower)
 284 ratios indicate NO_x-sensitive (saturated) conditions. Reductions in NO_x during the pandemic were
 285 substantial enough to shift the photochemical regime in some areas, *i.e.*, from NO_x-saturated to a
 286 transition zone or from a transition zone to NO_x-sensitive conditions (Peralta et al., 2021). The SI contains
 a version of Table 1 that also includes tropospheric column HCHO:NO₂ ratios over each city. We did not

287 identify a consistent relationship between this ratio and the sensitivity of PAN to COVID induced-
288 changes to NO_x.

289 PANs decreased significantly over LA during COVID-19 NO_x emission reductions, and this
290 coincided with decreases in surface O₃ (Connerton et al., 2020; Schroeder et al., 2022). The underlying
291 photochemical environment of LA has been transitioning from a VOC-limited regime to a NO_x-limited
292 regime (Lee et al., 2021; Schroeder et al., 2022); spring 2020 was the first NO_x-limited year (Schroeder et
293 al., 2022). PAN abundances at the ground have decreased much more rapidly than O₃ in response to
294 emission controls in the LA Basin (Pollack et al., 2013). The CrIS data suggest that PAN would continue
295 to respond to NO_x emission reductions in this city.

296 PANs did not show marked changes over Mexico City, São Paulo or Tokyo despite major NO_x
297 perturbations. O₃ over Tokyo also did not significantly change with COVID-19 lockdown measures; this
298 has been attributed to a shift in the underlying photochemical regime from VOC-limited towards the
299 transition zone where O₃ production is expected to be equally sensitive to changes in both NO_x and VOCs
300 (Damiani et al., 2022; Ito et al., 2021; Q. Wang & Li, 2021). O₃ in Mexico City was also statistically
301 indistinguishable during periods of substantial precursor reduction in 2020 from that of other years
302 (Peralta et al., 2021). São Paulo experienced an increase in O₃ in April and May, but largely in areas most
303 seriously impacted by vehicle emissions (Alvim et al., 2023).

304 The largest and only significant increase in free tropospheric PANs on a monthly mean scale in
305 our analysis occurred over Beijing in January (80%, $p = 0.03$), coincident with the lowest average HCHO:
306 NO₂ ratio of all cities included here. Qiu et al. (2020) reported a threefold increase in ground-level PAN
307 in urban Beijing during this first lockdown period, connected to enhanced local photochemistry and
308 abnormal meteorological conditions, including anomalous wind convergence under higher temperatures.
309 We find a similar change in free tropospheric PANs over Beijing, where mean CrIS PANs are 2.4 times
310 higher during the same lockdown period. Beijing had a second period of NO₂ decline in July and August
311 2020, which was associated with an insignificant change in PANs (-1.96%, $p = 0.31$). Stavrakou et al.
312 (2021) also investigated the impact of COVID-19 on PAN over China.

313

314 **5 Conclusions**

315 We use CrIS data from 2016-2021 to identify the seasonality of PANs over 8 megacities, and identify
316 time periods with elevated PANs. This is the first detailed analysis of satellite observations of PANs over
317 multiple megacities. We use this to inform our analysis in diagnosing the impact of NO₂ declines related
318 to the COVID-19 pandemic on PANs in these locations.

319

320

321 1. There are pronounced seasonal cycles in PANs over each megacity. Monthly mean PANs peak in
322 the spring or summer (Beijing and Karachi), aligning with respective seasonal maximums in
323 photochemical activity. Wildfire smoke can occasionally enhance monthly mean PANs.

324

325

326 2. Despite large changes in tropospheric NO₂ columns associated with the COVID-19 pandemic, we
327 only identify two megacities over which PANs changed significantly: Beijing and LA. The
328 relative response of PANs in these locations was smaller than the changes in NO₂. The response
329 of PANs to a major change in precursor emissions is highly non-linear.

330

331

332 3. Sensitivity of free tropospheric PANs to the abundance of precursors appears to be seasonally
333 dependent in Beijing and Tokyo. PANs over Beijing and Tokyo are likely more sensitive to NO_x
334 reductions in winter and spring respectively.

335
336
337
338
339
340
341

4. Based on this survey of megacities, relatively large perturbations in NO_x may not result in significant declines in NO_x export potential of megacities in all seasons. Thus satellite observations of PANs may be an additional useful diagnostic in predicting the complex response of O₃ to NO_x reductions in downwind regions. Next steps should focus on identifying the response of PAN downwind of megacities to COVID-19 NO_x reductions.

342 **Acknowledgments**

343 This work is funded under NASA award no. 80NSSC20K0947. Part of this work was carried out
344 at the Jet Propulsion Laboratory, California Institute of Technology, under a contract with the
345 National Aeronautics and Space Administration (80NM0018D0004). We thank Isabelle De
346 Smedt and Folkert Boersma for collaborating on the proposal that led to this work and for
347 answering questions regarding the OMI data.

348

349 **Open Research**

350 The Summary and Standard Product of CrIS PANs megacity Special Collection data for each
351 megacity used in this study are available online through the Goddard Earth Sciences Data and
352 Information services Center (NASA GES DISC) (Bowman, 2021c, 2021k, 2021g, 2021o, 2021a,
353 2021e, 2021m, 2021i, 2021l, 2021h, 2021p, 2021d, 2021n, 2021j, 2021b, 2021f, 2021c). Megacity
354 datasets for Lagos and São Paulo can be found at <https://doi.org/10.5061/dryad.wpzgmsbtk> and
355 eventually on the NASA GES DISC. OMI NO₂ and HCHO data were obtained from
356 <https://www.temis.nl/airpollution/no2.php> and <https://h2co.aeronomie.be/> (last access: August 2021),
357 (Boersma et al., 2017b; De Smedt et al., 2017).

358
359

360

361

362

363

364

365

366

367

368

369 **References**

- 370 Abdul Raheem, A. M. O., Adekola, F. A., & Obioh, I. O. (2009). The Seasonal Variation of the
 371 Concentrations of Ozone, Sulfur Dioxide, and Nitrogen Oxides in Two Nigerian Cities.
 372 *Environmental Modeling & Assessment*, *14*(4), 497–509. [https://doi.org/10.1007/s10666-](https://doi.org/10.1007/s10666-008-9142-x)
 373 [008-9142-x](https://doi.org/10.1007/s10666-008-9142-x)
- 374 Alvarado, M. J., Cady-Pereira, K. E., Xiao, Y., Millet, D. B., & Payne, V. H. (2011). Emission
 375 Ratios for Ammonia and Formic Acid and Observations of Peroxy Acetyl Nitrate (PAN)
 376 and Ethylene in Biomass Burning Smoke as Seen by the Tropospheric Emission
 377 Spectrometer (TES). *Atmosphere*, *2*(4), 633–654. <https://doi.org/10.3390/atmos2040633>
- 378 Alvim, D. S., Herdies, D. L., Corrêa, S. M., Basso, L. S., Khalid, B., Silva, G. F. P., Oyerinde,
 379 G., De Carvalho, N. A., Coelho, S. M. S. D. C., & Figueroa, S. N. (2023). COVID-19
 380 Pandemic: Impacts on Air Quality during Partial Lockdown in the Metropolitan Area of
 381 São Paulo. *Remote Sensing*, *15*(5), 1262. <https://doi.org/10.3390/rs15051262>
- 382 Bauwens, M., Compernelle, S., Stavrou, T., Müller, J. -F., Gent, J., Eskes, H., Levelt, P. F., A,
 383 R., Veefkind, J. P., Vlietinck, J., Yu, H., & Zehner, C. (2020). Impact of Coronavirus
 384 Outbreak on NO₂ Pollution Assessed Using TROPOMI and OMI Observations.
 385 *Geophysical Research Letters*, *47*(11). <https://doi.org/10.1029/2020GL087978>
- 386 Berman, J. D., & Ebisu, K. (2020). Changes in U.S. air pollution during the COVID-19
 387 pandemic. *Science of The Total Environment*, *739*, 139864.
 388 <https://doi.org/10.1016/j.scitotenv.2020.139864>
- 389 Boersma, K. F., Eskes, H. J., Richter, A., De Smedt, I., Lorente, A., Beirle, S., van Geffen, J. H.
 390 G. M., Zara, M., Peters, E., Van Roozendaal, M., Wagner, T., Maasakkers, J. D., van der
 391 A, R. J., Nightingale, J., De Rudder, A., Irie, H., Pinardi, G., Lambert, J.-C., &

- 392 Compernelle, S. C. (2018). Improving algorithms and uncertainty estimates for satellite
393 NO₂ retrievals: Results from the quality assurance for the
394 essential climate variables (QA4ECV) project. *Atmospheric Measurement Techniques*,
395 *11*(12), 6651–6678. <https://doi.org/10.5194/amt-11-6651-2018>
- 396 Boersma, K. F., Eskes, H., Richter, A., De Smedt, I., Lorente, A., Beirle, S., van Geffen, J. H. G.
397 M., Peters, E., Van Roozendael, M., & Wagner, T. (2017a). *QA4ECV NO₂ tropospheric*
398 *and stratospheric vertical column data from GOME-2A (Version 1.1) [Data set]*. Royal
399 Netherlands Meteorological Institute (KNMI). [http://doi.org/10.21944/qa4ecv-no2-](http://doi.org/10.21944/qa4ecv-no2-gome2a-v1.1)
400 [gome2a-v1.1](http://doi.org/10.21944/qa4ecv-no2-gome2a-v1.1)
- 401 Boersma, K. F., Eskes, H., Richter, A., De Smedt, I., Lorente, A., Beirle, S., van Geffen, J. H. G.
402 M., Peters, E., Van Roozendael, M., & Wagner, T. (2017b). *QA4ECV NO₂ tropospheric*
403 *and stratospheric vertical column data from OMI (Version 1.1) [Data set]*. Royal
404 Netherlands Meteorological Institute (KNMI). [http://doi.org/10.21944/qa4ecv-no2-omi-](http://doi.org/10.21944/qa4ecv-no2-omi-v1.1)
405 [v1.1](http://doi.org/10.21944/qa4ecv-no2-omi-v1.1)
- 406 Bowman, K. W. (2021a). *TROPESS CrIS-SNPP L2 Peroxyacetyl Nitrate for Beijing* (Standard
407 Product V1) [dataset]. Goddard Earth Sciences Data and Information Services Center
408 (GES DISC). <https://doi.org/10.5067/IUJHNI1MM1QA>
- 409 Bowman, K. W. (2021b). *TROPESS CrIS-SNPP L2 Peroxyacetyl Nitrate for Beijing* (Summary
410 Product V1) [dataset]. Goddard Earth Sciences Data and Information Services Center
411 (GES DISC). <https://doi.org/10.5067/GBMBES47TUOI>
- 412 Bowman, K. W. (2021c). *TROPESS CrIS-SNPP L2 Peroxyacetyl Nitrate for Delhi* (Standard
413 Product V1) [dataset]. Goddard Earth Sciences Data and Information Services Center
414 (GES DISC). <https://doi.org/10.5067/NILL9KD1K78G>

- 415 Bowman, K. W. (2021d). *TROPESS CrIS-SNPP L2 Peroxyacetyl Nitrate for Delhi* (Summary
416 Product V1) [dataset]. Goddard Earth Sciences Data and Information Services Center
417 (GES DISC). <https://doi.org/10.5067/IHXG5JVO98VC>
- 418 Bowman, K. W. (2021e). *TROPESS CrIS-SNPP L2 Peroxyacetyl Nitrate for Karachi* (Standard
419 Product V1) [dataset]. Goddard Earth Sciences Data and Information Services Center
420 (GES DISC). <https://doi.org/10.5067/3AKYF8OS8DHK>
- 421 Bowman, K. W. (2021f). *TROPESS CrIS-SNPP L2 Peroxyacetyl Nitrate for Karachi* (Summary
422 Product V1) [dataset]. Goddard Earth Sciences Data and Information Services Center
423 (GES DISC). <https://doi.org/OHZ38O337SMK>
- 424 Bowman, K. W. (2021g). *TROPESS CrIS-SNPP L2 Peroxyacetyl Nitrate for Lagos* (Standard
425 Product, V1) [dataset]. Goddard Earth Sciences Data and Information Services Center
426 (GES DISC). <https://doi.org/10.5067/4UH0WF2HOHHB>
- 427 Bowman, K. W. (2021h). *TROPESS CrIS-SNPP L2 Peroxyacetyl Nitrate for Lagos* (Summary
428 Product V1) [dataset]. Goddard Earth Sciences Data and Information Services Center
429 (GES DISC). <https://doi.org/10.5067/G2FKY92PRSF5>,
- 430 Bowman, K. W. (2021i). *TROPESS CrIS-SNPP L2 Peroxyacetyl Nitrate for Los Angeles*
431 (Standard Product V1) [dataset]. Goddard Earth Sciences Data and Information Services
432 Center (GES DISC). <https://doi.org/10.5067/0QPQFIXDET1X>
- 433 Bowman, K. W. (2021j). *TROPESS CrIS-SNPP L2 Peroxyacetyl Nitrate for Los Angeles*
434 (Summary Product V1) [dataset]. Goddard Earth Sciences Data and Information Services
435 Center (GES DISC). <https://doi.org/10.5067/H66DGC3ICJMQ>

- 436 Bowman, K. W. (2021k). *TROPESS CrIS-SNPP L2 Peroxyacetyl Nitrate for Mexico City*
437 (Standard Product V1) [dataset]. Goddard Earth Sciences Data and Information Services
438 Center (GES DISC). <https://doi.org/10.5067/PECEC1AZ5R1J>
- 439 Bowman, K. W. (2021l). *TROPESS CrIS-SNPP L2 Peroxyacetyl Nitrate for Mexico City*
440 (Summary Product V1) [dataset]. Goddard Earth Sciences Data and Information Services
441 Center (GES DISC). <https://doi.org/10.5067/YTO4AV07QQOW>
- 442 Bowman, K. W. (2021m). *TROPESS CrIS-SNPP L2 Peroxyacetyl Nitrate for São Paulo*
443 (Standard Product V1) [dataset]. Goddard Earth Sciences Data and Information Services
444 Center (GES DISC). <https://doi.org/10.5067/SQVOPBQTHU10>
- 445 Bowman, K. W. (2021n). *TROPESS CrIS-SNPP L2 Peroxyacetyl Nitrate for São Paulo*
446 (Summary Product V1) [dataset]. Goddard Earth Sciences Data and Information Services
447 Center (GES DISC). <https://doi.org/10.5067/AA26EWZUNMDK>
- 448 Bowman, K. W. (2021o). *TROPESS CrIS-SNPP L2 Peroxyacetyl Nitrate for Tokyo* (Standard
449 Product V1) [dataset]. Goddard Earth Sciences Data and Information Services Center
450 (GES DISC). <https://doi.org/10.5067/4UH0WF2HOHHB>
- 451 Bowman, K. W. (2021p). *TROPESS CrIS-SNPP L2 Peroxyacetyl Nitrate for Tokyo* (Summary
452 Product V1) [dataset]. Goddard Earth Sciences Data and Information Services Center
453 (GES DISC). <https://doi.org/10.5067/RAD13QSZ61JY>
- 454 Brice, K. A., Bottenheim, J. W., Anlauf, K. G., & Wiebe, H. A. (1988). Long-term
455 measurements of atmospheric peroxyacetyl nitrate (PAN) at rural sites in Ontario and
456 Nova Scotia; seasonal variations and long-range transport. *Tellus B*, 40B(5), 408–425.
457 <https://doi.org/10.1111/j.1600-0889.1988.tb00113.x>

- 458 Cady-Pereira, K. E., Payne, V. H., Neu, J. L., Bowman, K. W., Miyazaki, K., Marais, E. A.,
459 Kulawik, S., Tzompa-Sosa, Z. A., & Hegarty, J. D. (2017). Seasonal and spatial changes
460 in trace gases over megacities from Aura TES observations: Two case studies.
461 *Atmospheric Chemistry and Physics*, 17(15), 9379–9398. [https://doi.org/10.5194/acp-17-](https://doi.org/10.5194/acp-17-9379-2017)
462 9379-2017
- 463 Chinazzi, M., Davis, J. T., Ajelli, M., Gioannini, C., Litvinova, M., Merler, S., Pastore y Piontti,
464 A., Mu, K., Rossi, L., Sun, K., Viboud, C., Xiong, X., Yu, H., Halloran, M. E., Longini,
465 I. M., & Vespignani, A. (2020). The effect of travel restrictions on the spread of the 2019
466 novel coronavirus (COVID-19) outbreak. *Science*, 368(6489), 395–400.
467 <https://doi.org/10.1126/science.aba9757>
- 468 Clarisse, L., R'Honi, Y., Coheur, P.-F., Hurtmans, D., & Clerbaux, C. (2011). Thermal infrared
469 nadir observations of 24 atmospheric gases: TRACE GAS OBSERVATIONS FROM
470 IASI. *Geophysical Research Letters*, 38(10), n/a-n/a.
471 <https://doi.org/10.1029/2011GL047271>
- 472 Coggon, M. M., Gkatzelis, G. I., McDonald, B. C., Gilman, J. B., Schwantes, R. H., Abuhassan,
473 N., Aikin, K. C., Arend, M. F., Berkoff, T. A., Brown, S. S., Campos, T. L., Dickerson,
474 R. R., Gronoff, G., Hurley, J. F., Isaacman-VanWertz, G., Koss, A. R., Li, M., McKeen,
475 S. A., Moshary, F., ... Warneke, C. (2021). Volatile chemical product emissions enhance
476 ozone and modulate urban chemistry. *Proceedings of the National Academy of Sciences*,
477 118(32), e2026653118. <https://doi.org/10.1073/pnas.2026653118>
- 478 Connerton, P., Vicente de Assunção, J., Maura de Miranda, R., Dorothée Slovic, A., José Pérez-
479 Martínez, P., & Ribeiro, H. (2020). Air Quality during COVID-19 in Four Megacities:

- 480 Lessons and Challenges for Public Health. *International Journal of Environmental*
481 *Research and Public Health*, 17(14), 5067. <https://doi.org/10.3390/ijerph17145067>
- 482 Damiani, A., Irie, H., Belikov, D. A., Kaizuka, S., Hoque, H. M. S., & Cordero, R. R. (2022).
483 Peculiar COVID-19 effects in the Greater Tokyo Area revealed by spatiotemporal
484 variabilities of tropospheric gases and light-absorbing aerosols. *Atmospheric Chemistry*
485 *and Physics*, 22(18), 12705–12726. <https://doi.org/10.5194/acp-22-12705-2022>
- 486 De Smedt, I., Müller, J.-F., Stavrou, T., van der A, R., Eskes, H., & Van Roozendaal, M.
487 (2008). Twelve years of global observations of formaldehyde in the troposphere using
488 GOME and SCIAMACHY sensors. *Atmospheric Chemistry and Physics*, 8(16), 4947–
489 4963. <https://doi.org/10.5194/acp-8-4947-2008>
- 490 De Smedt, I., Yu, H., Richter, A., Beirle, S., Eskes, H., Boersma, F., Van Roozendaal, M., van
491 Geffen, J. H. G. M., Lorente, A., & Peters, E. (2017). *QA4ECV HCHO tropospheric*
492 *column data from OMI (Version 1.1) [L3 Monthly Means]*. Royal Belgian Institute for
493 Space Aeronomy. <http://doi.org/10.18758/71021031>
- 494 Feng, X., Li, Q., Zhu, Y., Hou, J., Jin, L., & Wang, J. (2015). Artificial neural networks
495 forecasting of PM_{2.5} pollution using air mass trajectory based geographic model and
496 wavelet transformation. *Atmospheric Environment*, 107, 118–128.
497 <https://doi.org/10.1016/j.atmosenv.2015.02.030>
- 498 Fischer, E. V., Jacob, D. J., Yantosca, R. M., Sulprizio, M. P., Millet, D. B., Mao, J., Paulot, F.,
499 Singh, H. B., Roiger, A., Ries, L., Talbot, R. W., Dzepina, K., & Pandey Deolal, S.
500 (2014). Atmospheric peroxyacetyl nitrate (PAN): A global budget and source attribution.
501 *Atmospheric Chemistry and Physics*, 14(5), 2679–2698. [https://doi.org/10.5194/acp-14-](https://doi.org/10.5194/acp-14-2679-2014)
502 2679-2014

- 503 Fischer, E. V., Zhu, L., Payne, V. H., Worden, J. R., Jiang, Z., Kulawik, S. S., Brey, S.,
504 Hecobian, A., Gombos, D., Cady-Pereira, K., & Flocke, F. (2018). Using TES retrievals
505 to investigate PAN in North American biomass burning plumes. *Atmospheric Chemistry
506 and Physics*, 18(8), 5639–5653. <https://doi.org/10.5194/acp-18-5639-2018>
- 507 Franco, B., Clarisse, L., Stavrou, T., Müller, J. -F, Van Damme, M., Whitburn, S., Hadji-
508 Lazaro, J., Hurtmans, D., Taraborrelli, D., Clerbaux, C., & Coheur, P. -F. (2018). A
509 General Framework for Global Retrievals of Trace Gases From IASI: Application to
510 Methanol, Formic Acid, and PAN. *Journal of Geophysical Research: Atmospheres*,
511 123(24). <https://doi.org/10.1029/2018JD029633>
- 512 Fu, D., Bowman, K. W., Worden, H. M., Natraj, V., Worden, J. R., Yu, S., Veeffkind, P., Aben,
513 I., Landgraf, J., Strow, L., & Han, Y. (2016). High-resolution tropospheric carbon
514 monoxide profiles retrieved from CrIS and TROPOMI. *Atmospheric Measurement
515 Techniques*, 9(6), 2567–2579. <https://doi.org/10.5194/amt-9-2567-2016>
- 516 Gaffney, J. S., Marley, N. A., & Prestbo, E. W. (1989). Peroxyacyl Nitrates (PANs): Their
517 Physical and Chemical Properties. In O. Hutzinger (Ed.), *Air Pollution: Vol. 4 / 4B* (pp.
518 1–38). Springer Berlin Heidelberg. https://doi.org/10.1007/978-3-540-46113-5_1
- 519 Global Modeling and Assimilation Office (GMAO). (2015). *MERRA-2 tavgM_2d_slv_Nx:*
520 *2d, Monthly mean, Time-Averaged, Single-Level, Assimilation, Single-Level Diagnostics*
521 *V5.12.4*. Greenbelt, MD, USA, Goddard Earth Sciences Data and Information Services
522 Center (GES DISC). 10.5067/AP1B0BA5PD2K
- 523 Graedel, T. E., Bates, T. S., Bouwman, A. F., Cunnold, D., Dignon, J., Fung, I., Jacob, D. J.,
524 Lamb, B. K., Logan, J. A., Marland, G., Middleton, P., Pacyna, J. M., Placet, M., &

- 525 Veldt, C. (1993). A compilation of inventories of emissions to the atmosphere. *Global*
526 *Biogeochemical Cycles*, 7(1), 1–26. <https://doi.org/10.1029/92GB02793>
- 527 Gurjar, B. R., Ravindra, K., & Nagpure, A. S. (2016). Air pollution trends over Indian megacities
528 and their local-to-global implications. *Atmospheric Environment*, 142, 475–495.
529 <https://doi.org/10.1016/j.atmosenv.2016.06.030>
- 530 Honrath, R. E., Hamlin, A. J., & Merrill, J. T. (1996). Transport of ozone precursors from the
531 Arctic troposphere to the North Atlantic region. *Journal of Geophysical Research*,
532 101(D22), 29335–29351. <https://doi.org/10.1029/95JD02673>
- 533 Ito, A., Wakamatsu, S., Morikawa, T., & Kobayashi, S. (2021). 30 Years of Air Quality Trends
534 in Japan. *Atmosphere*, 12(8), 1072. <https://doi.org/10.3390/atmos12081072>
- 535 Janssens-Maenhout, G., Crippa, M., Guizzardi, D., Dentener, F., Muntean, M., Pouliot, G.,
536 Keating, T., Zhang, Q., Kurokawa, J., Wankmüller, R., Denier van der Gon, H., Kuenen,
537 J. J. P., Klimont, Z., Frost, G., Darras, S., Koffi, B., & Li, M. (2015). HTAP_v2.2: A
538 mosaic of regional and global emission grid maps for 2008 and 2010 to study
539 hemispheric transport of air pollution. *Atmospheric Chemistry and Physics*, 15(19),
540 11411–11432. <https://doi.org/10.5194/acp-15-11411-2015>
- 541 Jiang, Z., Worden, J. R., Payne, V. H., Zhu, L., Fischer, E., Walker, T., & Jones, D. B. A. (2016).
542 Ozone export from East Asia: The role of PAN. *Journal of Geophysical Research:*
543 *Atmospheres*, 121(11), 6555–6563. <https://doi.org/10.1002/2016JD024952>
- 544 Jin, X., Fiore, A. M., Murray, L. T., Valin, L. C., Lamsal, L. N., Duncan, B., Folkert Boersma,
545 K., De Smedt, I., Abad, G. G., Chance, K., & Tonnesen, G. S. (2017). Evaluating a
546 Space-Based Indicator of Surface Ozone-NO_x-VOC Sensitivity Over Midlatitude
547 Source Regions and Application to Decadal Trends: Space-Based Indicator of O₃

- 548 Sensitivity. *Journal of Geophysical Research: Atmospheres*, 122(19), 10,439-10,461.
549 <https://doi.org/10.1002/2017JD026720>
- 550 Juncosa Calahorrano, J. F., Payne, V. H., Kulawik, S., Ford, B., Flocke, F., Campos, T., &
551 Fischer, E. V. (2021). Evolution of Acyl Peroxynitrates (PANs) in Wildfire Smoke
552 Plumes Detected by the Cross-Track Infrared Sounder (CrIS) Over the Western U.S.
553 During Summer 2018. *Geophysical Research Letters*, 48(23).
554 <https://doi.org/10.1029/2021GL093405>
- 555 Langford, A. O., Senff, C. J., Alvarez, R. J., Banta, R. M., & Hardesty, R. M. (2010). Long-
556 range transport of ozone from the Los Angeles Basin: A case study: LONG-RANGE
557 TRANSPORT OF OZONE. *Geophysical Research Letters*, 37(6), n/a-n/a.
558 <https://doi.org/10.1029/2010GL042507>
- 559 Le, T., Wang, Y., Liu, L., Yang, J., Yung, Y. L., Li, G., & Seinfeld, J. H. (2020). Unexpected air
560 pollution with marked emission reductions during the COVID-19 outbreak in China.
561 *Science*, 369(6504), 702–706. <https://doi.org/10.1126/science.abb7431>
- 562 Lee, H.-J., Chang, L.-S., Jaffe, D. A., Bak, J., Liu, X., Abad, G. G., Jo, H.-Y., Jo, Y.-J., Lee, J.-
563 B., & Kim, C.-H. (2021). Ozone Continues to Increase in East Asia Despite Decreasing
564 NO₂: Causes and Abatements. *Remote Sensing*, 13(11), 2177.
565 <https://doi.org/10.3390/rs13112177>
- 566 Li, K., Jacob, D. J., Liao, H., Qiu, Y., Shen, L., Zhai, S., Bates, K. H., Sulprizio, M. P., Song, S.,
567 Lu, X., Zhang, Q., Zheng, B., Zhang, Y., Zhang, J., Lee, H. C., & Kuk, S. K. (2021).
568 Ozone pollution in the North China Plain spreading into the late-winter haze season.
569 *Proceedings of the National Academy of Sciences*, 118(10), e2015797118.
570 <https://doi.org/10.1073/pnas.2015797118>

- 571 Liang, Y., Sengupta, D., Campmier, M. J., Lunderberg, D. M., Apte, J. S., & Goldstein, A. H.
572 (2021). Wildfire smoke impacts on indoor air quality assessed using crowdsourced data
573 in California. *Proceedings of the National Academy of Sciences*, *118*(36), e2106478118.
574 <https://doi.org/10.1073/pnas.2106478118>
- 575 Liu, T., Chen, G., Chen, J., Xu, L., Li, M., Hong, Y., Chen, Y., Ji, X., Yang, C., Chen, Y.,
576 Huang, W., Huang, Q., & Wang, H. (2022). Seasonal characteristics of atmospheric
577 peroxyacetyl nitrate (PAN) in a coastal city of Southeast China: Explanatory factors and
578 photochemical effects. *Atmospheric Chemistry and Physics*, *22*(7), 4339–4353.
579 <https://doi.org/10.5194/acp-22-4339-2022>
- 580 Liu, Z., Ciais, P., Deng, Z., Lei, R., Davis, S. J., Feng, S., Zheng, B., Cui, D., Dou, X., He, P.,
581 Zhu, B., Lu, C., Ke, P., Sun, T., Yue, X., Wang, Y., Lei, Y., Zhou, H., Cai, Z., ...
582 Schellnhuber, H. J. (n.d.). *Near-real-time data captured record decline in global CO2*
583 *emissions due to COVID-19*. 45.
- 584 Liu, Z., Wang, Y., Gu, D., Zhao, C., Huey, L. G., Stickel, R., Liao, J., Shao, M., Zhu, T., Zeng,
585 L., Liu, S.-C., Chang, C.-C., Amoroso, A., & Costabile, F. (2010). Evidence of Reactive
586 Aromatics As a Major Source of Peroxy Acetyl Nitrate over China. *Environmental*
587 *Science & Technology*, *44*(18), 7017–7022. <https://doi.org/10.1021/es1007966>
- 588 Martin, R. V., Fiore, A. M., & Van Donkelaar, A. (2004). Space-based diagnosis of surface
589 ozone sensitivity to anthropogenic emissions: SURFACE OZONE SENSITIVITY TO
590 EMISSIONS. *Geophysical Research Letters*, *31*(6), n/a-n/a.
591 <https://doi.org/10.1029/2004GL019416>
- 592 Mena-Carrasco, M., Carmichael, G. R., Campbell, J. E., Zimmerman, D., Tang, Y., Adhikary,
593 B., D'allura, A., Molina, L. T., Zavala, M., Garcia, A., Flocke, F., Campos, T.,

- 594 Weinheimer, A. J., Shetter, R., Apel, E., Montzka, D. D., Knapp, D. J., & Zheng, W.
595 (2009). Assessing the regional impacts of Mexico City emissions on air quality and
596 chemistry. *Atmos. Chem. Phys.*, 13.
- 597 Miyazaki, K., Bowman, K., Sekiya, T., Eskes, H., Boersma, F., Worden, H., Livesey, N., Payne,
598 V. H., Sudo, K., Kanaya, Y., Takigawa, M., & Ogochi, K. (2020). Updated tropospheric
599 chemistry reanalysis and emission estimates, TCR-2, for 2005–2018. *Earth System
600 Science Data*, 12(3), 2223–2259. <https://doi.org/10.5194/essd-12-2223-2020>
- 601 Miyazaki, K., Bowman, K., Sekiya, T., Jiang, Z., Chen, X., Eskes, H., Ru, M., Zhang, Y., &
602 Shindell, D. (2020). Air Quality Response in China Linked to the 2019 Novel
603 Coronavirus (COVID-19) Lockdown. *Geophysical Research Letters*, 47(19).
604 <https://doi.org/10.1029/2020GL089252>
- 605 Miyazaki, K., Bowman, K., Sekiya, T., Takigawa, M., Neu, J. L., Sudo, K., Osterman, G., &
606 Eskes, H. (2021). Global tropospheric ozone responses to reduced NO_x emissions linked
607 to the COVID-19 worldwide lockdowns. *SCIENCE ADVANCES*, 15.
- 608 Miyazaki, K., Eskes, H., Sudo, K., Boersma, K. F., Bowman, K., & Kanaya, Y. (2017). Decadal
609 changes in global surface NO₂; emissions from multi-constituent satellite data
610 assimilation. *Atmospheric Chemistry and Physics*, 17(2), 807–837.
611 <https://doi.org/10.5194/acp-17-807-2017>
- 612 Nussbaumer, C. M., & Cohen, R. C. (2020). The Role of Temperature and NO_x in Ozone
613 Trends in the Los Angeles Basin. *Environmental Science & Technology*, 54(24), 15652–
614 15659. <https://doi.org/10.1021/acs.est.0c04910>
- 615 Odekanle, E. L., Fakinle, B. S., Odejobi, O. J., Akangbe, O. E., Sonibare, J. A., Akeredolu, F. A.,
616 & Oladoja, O. M. (2022). COVID-19 induced restriction in developing countries and its

- 617 impacts on pollution load: Case study of Lagos mega city. *Heliyon*, 8(8), e10402.
618 <https://doi.org/10.1016/j.heliyon.2022.e10402>
- 619 Payne, V. H., Alvarado, M. J., Cady-Pereira, K. E., Worden, J. R., Kulawik, S. S., & Fischer, E.
620 V. (2014). Satellite observations of peroxyacetyl nitrate from the Aura Tropospheric
621 Emission Spectrometer. *Atmospheric Measurement Techniques*, 7(11), 3737–3749.
622 <https://doi.org/10.5194/amt-7-3737-2014>
- 623 Payne, V. H., Fischer, E. V., Worden, J. R., Jiang, Z., Zhu, L., Kurosu, T. P., & Kulawik, S. S.
624 (2017). Spatial variability in tropospheric peroxyacetyl nitrate in the tropics from infrared
625 satellite observations in 2005 and 2006. *Atmospheric Chemistry and Physics*, 17(10),
626 6341–6351. <https://doi.org/10.5194/acp-17-6341-2017>
- 627 Payne, V. H., Kulawik, S. S., Fischer, E. V., Brewer, J. F., Huey, L. G., Miyazaki, K., Worden, J.
628 R., Bowman, K. W., Hints, E. J., Moore, F., Elkins, J. W., & Juncosa Calahorrano, J.
629 (2022). *Satellite measurements of peroxyacetyl nitrate from the Cross-Track Infrared*
630 *Sounder: Comparison with ATom aircraft measurements. Gases/Remote*
631 *Sensing/Validation and Intercomparisons.* <https://doi.org/10.5194/amt-15-3497-2022>
- 632 Penkett, S. A., & Brice, K. A. (1986). The spring maximum in photo-oxidants in the Northern
633 Hemisphere troposphere. *Nature*, 319(6055), 655–657. <https://doi.org/10.1038/319655a0>
- 634 Peralta, O., Ortíz-Alvarez, A., Torres-Jardón, R., Suárez-Lastra, M., Castro, T., & Ruíz-
635 Suárez, L. G. (2021). Ozone over Mexico City during the COVID-19 pandemic. *Science*
636 *of The Total Environment*, 761, 143183. <https://doi.org/10.1016/j.scitotenv.2020.143183>
- 637 Pollack, I. B., Ryerson, T. B., Trainer, M., Neuman, J. A., Roberts, J. M., & Parrish, D. D.
638 (2013). Trends in ozone, its precursors, and related secondary oxidation products in Los
639 Angeles, California: A synthesis of measurements from 1960 to 2010: OZONE TRENDS

- 640 IN LA FROM 1960 TO 2010. *Journal of Geophysical Research: Atmospheres*, 118(11),
641 5893–5911. <https://doi.org/10.1002/jgrd.50472>
- 642 Qiu, Y., Ma, Z., & Li, K. (2019). A modeling study of the peroxyacetyl nitrate (PAN) during a
643 wintertime haze event in Beijing, China. *Science of The Total Environment*, 650, 1944–
644 1953. <https://doi.org/10.1016/j.scitotenv.2018.09.253>
- 645 Qiu, Y., Ma, Z., Li, K., Lin, W., Tang, Y., Dong, F., & Liao, H. (2020). Markedly Enhanced
646 Levels of Peroxyacetyl Nitrate (PAN) During COVID-19 in Beijing. *Geophysical
647 Research Letters*, 47(19). <https://doi.org/10.1029/2020GL089623>
- 648 Randerson, J., van der verf, G., Gilglio, L., Collatz, G., & Kasibhatla, P. (2018). Global Fire
649 Emissions Database, Version 4, (GFEDv4), ORNL DAAC. *Oak Ridge, Tennessee, USA*.
- 650 Rappenglück, B., Melas, D., & Fabian, P. (2003). Evidence of the impact of urban plumes on
651 remote sites in the Eastern Mediterranean. *Atmospheric Environment*, 37(13), 1853–
652 1864. [https://doi.org/10.1016/S1352-2310\(03\)00065-7](https://doi.org/10.1016/S1352-2310(03)00065-7)
- 653 Roberts, J. M. (2007). PAN and Related Compounds. In R. Koppmann (Ed.), *Volatile Organic
654 Compounds in the Atmosphere* (pp. 221–268). Blackwell Publishing Ltd.
655 <https://doi.org/10.1002/9780470988657.ch6>
- 656 Saxena, P., Sonwani, S., Srivastava, A., Jain, M., Srivastava, A., Bharti, A., Rangra, D., Mongia,
657 N., Tejan, S., & Bhardwaj, S. (2021). Impact of crop residue burning in Haryana on the
658 air quality of Delhi, India. *Heliyon*, 7(5), e06973.
659 <https://doi.org/10.1016/j.heliyon.2021.e06973>
- 660 Schroeder, J. R., Cai, C., Xu, J., Ridley, D., Lu, J., Bui, N., Yan, F., & Avise, J. (2022).
661 Changing ozone sensitivity in the South Coast Air Basin during the COVID-19 period.

- 662 *Atmospheric Chemistry and Physics*, 22(19), 12985–13000. <https://doi.org/10.5194/acp->
663 22-12985-2022
- 664 Sharma, S., Zhang, M., Anshika, Gao, J., Zhang, H., & Kota, S. H. (2020). Effect of restricted
665 emissions during COVID-19 on air quality in India. *Science of The Total Environment*,
666 728, 138878. <https://doi.org/10.1016/j.scitotenv.2020.138878>
- 667 Shen, L., Jacob, D. J., Zhu, L., Zhang, Q., Zheng, B., Sulprizio, M. P., Li, K., De Smedt, I.,
668 González Abad, G., Cao, H., Fu, T., & Liao, H. (2019). The 2005–2016 Trends of
669 Formaldehyde Columns Over China Observed by Satellites: Increasing Anthropogenic
670 Emissions of Volatile Organic Compounds and Decreasing Agricultural Fire Emissions.
671 *Geophysical Research Letters*, 46(8), 4468–4475. <https://doi.org/10.1029/2019GL082172>
- 672 Shi, X., & Brasseur, G. P. (2020). The Response in Air Quality to the Reduction of Chinese
673 Economic Activities During the COVID-19 Outbreak. *Geophysical Research Letters*,
674 47(11). <https://doi.org/10.1029/2020GL088070>
- 675 Shogrin, M. J. (2023). *CrIS PANs megacity dataset for São Paulo and Lagos* [..Csv]. Dryad.
676 <https://doi.org/10.5061/dryad.wpzgmsbtk>
- 677 Shogrin, M. J., Payne, V. H., Kulawik, S. S., Miyazaki, K., & Fischer, E. V. (2023).
678 Measurement report: Spatiotemporal variability of peroxy acyl nitrates (PANs) over
679 Mexico City from TES and CrIS satellite measurements. *Atmospheric Chemistry and*
680 *Physics*, 23(4), 2667–2682. <https://doi.org/10.5194/acp-23-2667-2023>
- 681 Sicard, P., De Marco, A., Agathokleous, E., Feng, Z., Xu, X., Paoletti, E., Rodriguez, J. J. D., &
682 Calatayud, V. (2020). Amplified ozone pollution in cities during the COVID-19
683 lockdown. *Science of The Total Environment*, 735, 139542.
684 <https://doi.org/10.1016/j.scitotenv.2020.139542>

- 685 Sillman, S., & West, J. J. (2009). Reactive nitrogen in Mexico City and its relation to ozone-
686 precursor sensitivity: Results from photochemical models. *Atmos. Chem. Phys.*, 13.
- 687 Singh, H. B., & Hanst, P. L. (1981). Peroxyacetyl nitrate (PAN) in the unpolluted atmosphere:
688 An important reservoir for nitrogen oxides. *Geophysical Research Letters*, 8(8), 941–944.
689 <https://doi.org/10.1029/GL008i008p00941>
- 690 Singh, H. B., Salas, L. J., & Viezee, W. (1986). Global distribution of peroxyacetyl nitrate.
691 *Nature*, 321(6070), 588–591. <https://doi.org/10.1038/321588a0>
- 692 Souri, A. H., Johnson, M. S., Wolfe, G. M., Crawford, J. H., Fried, A., Wisthaler, A., Brune, W.
693 H., Blake, D. R., Weinheimer, A. J., Verhoelst, T., Compernelle, S., Pinardi, G.,
694 Vigouroux, C., Langerock, B., Choi, S., Lamsal, L., Zhu, L., Sun, S., Cohen, R. C., ...
695 Chance, K. (2023). Characterization of errors in satellite-based HCHO/NO₂
696 tropospheric column ratios with respect to chemistry, column-to-PBL translation, spatial
697 representation, and retrieval uncertainties. *Atmospheric Chemistry and Physics*, 23(3),
698 1963–1986. <https://doi.org/10.5194/acp-23-1963-2023>
- 699 Souri, A. H., Nowlan, C. R., Wolfe, G. M., Lamsal, L. N., Chan Miller, C. E., Abad, G. G., Janz,
700 S. J., Fried, A., Blake, D. R., Weinheimer, A. J., Diskin, G. S., Liu, X., & Chance, K.
701 (2020). Revisiting the effectiveness of HCHO/NO₂ ratios for inferring ozone sensitivity
702 to its precursors using high resolution airborne remote sensing observations in a high
703 ozone episode during the KORUS-AQ campaign. *Atmospheric Environment*, 224,
704 117341. <https://doi.org/10.1016/j.atmosenv.2020.117341>
- 705 Stavrakou, T., Müller, J.-F., Bauwens, M., Doumbia, T., Elguindi, N., Darras, S., Granier, C.,
706 Smedt, I. D., Lerot, C., Van Roozendaal, M., Franco, B., Clarisse, L., Clerbaux, C.,
707 Coheur, P.-F., Liu, Y., Wang, T., Shi, X., Gaubert, B., Tilmes, S., & Brasseur, G. (2021).

- 708 Atmospheric Impacts of COVID-19 on NO_x and VOC Levels over China Based on
709 TROPOMI and IASI Satellite Data and Modeling. *Atmosphere*, 12(8), 946.
710 <https://doi.org/10.3390/atmos12080946>
- 711 Steiner, A. L., Davis, A. J., Sillman, S., Owen, R. C., Michalak, A. M., & Fiore, A. M. (2010).
712 Observed suppression of ozone formation at extremely high temperatures due to chemical
713 and biophysical feedbacks. *Proceedings of the National Academy of Sciences*, 107(46),
714 19685–19690. <https://doi.org/10.1073/pnas.1008336107>
- 715 Venter, Z. S., Aunan, K., Chowdhury, S., & Lelieveld, J. (2020). COVID-19 lockdowns cause
716 global air pollution declines. *Proceedings of the National Academy of Sciences*, 117(32),
717 18984–18990. <https://doi.org/10.1073/pnas.2006853117>
- 718 Wang, L., Jin, X., Wang, Q., Mao, H., Liu, Q., Weng, G., & Wang, Y. (2020). Spatial and
719 temporal variability of open biomass burning in Northeast China from 2003 to 2017.
720 *Atmospheric and Oceanic Science Letters*, 13(3), 240–247.
721 <https://doi.org/10.1080/16742834.2020.1742574>
- 722 Wang, Q., & Li, S. (2021). Nonlinear impact of COVID-19 on pollutions – Evidence from
723 Wuhan, New York, Milan, Madrid, Bandra, London, Tokyo and Mexico City.
724 *Sustainable Cities and Society*, 65, 102629. <https://doi.org/10.1016/j.scs.2020.102629>
- 725 Warneke, C., de Gouw, J. A., Edwards, P. M., Holloway, J. S., Gilman, J. B., Kuster, W. C.,
726 Graus, M., Atlas, E., Blake, D., Gentner, D. R., Goldstein, A. H., Harley, R. A., Alvarez,
727 S., Rappenglueck, B., Trainer, M., & Parrish, D. D. (2013). Photochemical aging of
728 volatile organic compounds in the Los Angeles basin: Weekday-weekend effect: VOC
729 WEEKDAY-WEEKEND EFFECT. *Journal of Geophysical Research: Atmospheres*,
730 118(10), 5018–5028. <https://doi.org/10.1002/jgrd.50423>

- 731 WHO. (2020). *Coronavirus disease 2019 (COVID-19): Situation Report – 43*.
732 [www.who.int/docs/default-source/coronaviruse/situation-reports/20200303-sitrep-43-](http://www.who.int/docs/default-source/coronaviruse/situation-reports/20200303-sitrep-43-covid-19.pdf?sfvrsn=2c21c09c_2)
733 [covid-19.pdf?sfvrsn=2c21c09c_2](http://www.who.int/docs/default-source/coronaviruse/situation-reports/20200303-sitrep-43-covid-19.pdf?sfvrsn=2c21c09c_2).
- 734 Worden, H. M., Francis, G. L., Kulawik, S. S., Bowman, K. W., Cady-Pereira, K., Fu, D.,
735 Hegarty, J. D., Kantchev, V., Luo, M., Payne, V. H., Worden, J. R., Commane, R., &
736 McKain, K. (2022). *TROPES/CrIS carbon monoxide profile validation with NOAA*
737 *GML and ATom in situ aircraft observations* [Preprint]. Gases/Remote
738 Sensing/Validation and Intercomparisons. <https://doi.org/10.5194/amt-2022-128>
- 739 Yin, L., Du, P., Zhang, M., Liu, M., Xu, T., & Song, Y. (2019). Estimation of emissions from
740 biomass burning in China (2003–2017) based on MODIS fire radiative energy data.
741 *Biogeosciences*, *16*(7), 1629–1640. <https://doi.org/10.5194/bg-16-1629-2019>
- 742 Yoshitomi, M., Wild, O., & Akimoto, H. (2011). *Contributions of regional and intercontinental*
743 *transport to surface ozone in Tokyo* [Preprint]. Gases/Atmospheric
744 Modelling/Troposphere/Chemistry (chemical composition and reactions).
745 <https://doi.org/10.5194/acpd-11-10403-2011>
- 746 Zhang, B., Zhao, B., Zuo, P., Huang, Z., & Zhang, J. (2017). Ambient peroxyacyl nitrate
747 concentration and regional transportation in Beijing. *Atmospheric Environment*, *166*,
748 543–550. <https://doi.org/10.1016/j.atmosenv.2017.07.053>
- 749 Zhang, B., Zhao, X., & Zhang, J. (2019). Characteristics of peroxyacetyl nitrate pollution during
750 a 2015 winter haze episode in Beijing. *Environmental Pollution*, *244*, 379–387.
751 <https://doi.org/10.1016/j.envpol.2018.10.078>
- 752 Zhang, G., Mu, Y., Zhou, L., Zhang, C., Zhang, Y., Liu, J., Fang, S., & Yao, B. (2015a).
753 Summertime distributions of peroxyacetyl nitrate (PAN) and peroxypropionyl nitrate

- 754 (PPN) in Beijing: Understanding the sources and major sink of PAN. *Atmospheric*
755 *Environment*, 103, 289–296. <https://doi.org/10.1016/j.atmosenv.2014.12.035>
- 756 Zhang, G., Mu, Y., Zhou, L., Zhang, C., Zhang, Y., Liu, J., Fang, S., & Yao, B. (2015b).
757 Summertime distributions of peroxyacetyl nitrate (PAN) and peroxypropionyl nitrate
758 (PPN) in Beijing: Understanding the sources and major sink of PAN. *Atmospheric*
759 *Environment*, 103, 289–296. <https://doi.org/10.1016/j.atmosenv.2014.12.035>
- 760 Zhang, G., Xia, L., Zang, K., Xu, W., Zhang, F., Liang, L., Yao, B., Lin, W., & Mu, Y. (2020).
761 The abundance and inter-relationship of atmospheric peroxyacetyl nitrate (PAN),
762 peroxypropionyl nitrate (PPN), O₃, and NO_y during the wintertime in Beijing, China.
763 *Science of The Total Environment*, 718, 137388.
764 <https://doi.org/10.1016/j.scitotenv.2020.137388>
- 765 Zhang, J., Lim, Y.-H., Andersen, Z. J., Napolitano, G., Taghavi Shahri, S. M., So, R., Plucker,
766 M., Danesh-Yazdi, M., Cole-Hunter, T., Therning Jørgensen, J., Liu, S., Bergmann, M.,
767 Jayant Mehta, A., H. Mortensen, L., Requia, W., Lange, T., Loft, S., Kuenzli, N.,
768 Schwartz, J., & Amini, H. (2022). Stringency of COVID-19 Containment Response
769 Policies and Air Quality Changes: A Global Analysis across 1851 Cities. *Environmental*
770 *Science & Technology*, 56(17), 12086–12096. <https://doi.org/10.1021/acs.est.2c04303>
- 771 Zhao, Y., Xu, R., Xu, Z., Wang, L., & Wang, P. (2022). Temporal and Spatial Patterns of
772 Biomass Burning Fire Counts and Carbon Emissions in the Beijing–Tianjin–Hebei
773 (BTH) Region during 2003–2020 Based on GFED4. *Atmosphere*, 13(3), 459.
774 <https://doi.org/10.3390/atmos13030459>
- 775 Zhu, L., Fischer, E. V., Payne, V. H., Worden, J. R., & Jiang, Z. (2015). TES observations of the
776 interannual variability of PAN over Northern Eurasia and the relationship to springtime

777 fires. *Geophysical Research Letters*, 42(17), 7230–7237.

778 <https://doi.org/10.1002/2015GL065328>

779 Zhu, L., Payne, V. H., Walker, T. W., Worden, J. R., Jiang, Z., Kulawik, S. S., & Fischer, E. V.

780 (2017). PAN in the eastern Pacific free troposphere: A satellite view of the sources,

781 seasonality, interannual variability, and timeline for trend detection. *Journal of*

782 *Geophysical Research: Atmospheres*, 122(6), 3614–3629.

783 <https://doi.org/10.1002/2016JD025868>

784